EOO Report 95-008

Final Report

Coastal Water Optical Properties Prediction Development

CONTRACT N00014-93-C-0155

by

DONALD LEONARD, THOMAS DRISCOLL, AND PAUL TITTERTON

NOVEMBER 1995

prepared for

OFFICE OF NAVAL RESEARCH
ARLINGTON, VIRGINIA

The Electro-Optics Organization

269 North Mathilda Avenue, P.O. Box 60339, Sunnyvale, CA 94088
408 738 5390 Fax: 408 738 5399 e-mail: EOOinc @ aol.com

DISCLAIMER NOTICE

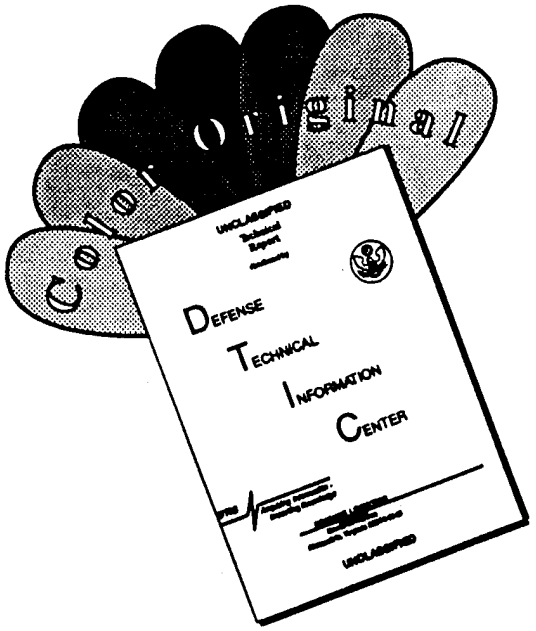

THIS DOCUMENT IS BEST QUALITY AVAILABLE. THE COPY FURNISHED TO DTIC CONTAINED A SIGNIFICANT NUMBER OF COLOR PAGES WHICH DO NOT REPRODUCE LEGIBLY ON BLACK AND WHITE MICROFICHE.

REPORT DOCUMENTATION PAGE

Form Approved
OMB No. 0704-0188

1. AGENCY USE ONLY (*Leave blank*)	2. REPORT DATE	3. REPORT TYPE AND DATES COVERED
	22 Nov 1995	Final 93 Mar. to 95 Aug.

4. TITLE AND SUBTITLE

Final Technical Report; Contract N00014-93-C-0155
Coastal Water Optical Properties Prediction Development

5. FUNDING NUMBERS

6. AUTHOR(S)

Donald Leonard, Thomas Driscoll, and Paul Titterton

7. PERFORMING ORGANIZATION NAME(S) AND ADDRESS(ES)

EOO, Inc.
269 N. Mathilda Ave.
Sunnyvale, CA 94086

8. PERFORMING ORGANIZATION REPORT NUMBER

EOO Report 95-008

9. SPONSORING / MONITORING AGENCY NAME(S) AND ADDRESS(ES)

Office of Naval Research
800 N. Quincy St.
Arlington, VA 22217

10. SPONSORING / MONITORING AGENCY REPORT NUMBER

11. SUPPLEMENTARY NOTES

The views and conclusions contained in this document are those of the authors and should not be interpreted as necessarily representing the official policy of the United States Government.

12a. DISTRIBUTION/ AVAILABILITY STATEMENT

Unlimited

12b. DISTRIBUTION CODE

13. ABSTRACT (*Maximum 200 words*)

Remote sensing concepts were evaluated for providing initial conditions to the Coastal Water Clarity predictive model. The most important water physical properties that strongly influence water optical properties are the concentrations of chlorophyll, sediment and dissolved organic matter. The currently available satellite multispectral imaging sensors do not have the required high sensitivity and small pixel size to be useful as a coastal water reconnaissance sensor. Two new satellite sensor concepts were developed to improve satellite capability. One concept uses a narrow swath sensor array with time delayed integration. The second concept utilizes a shot-noise limited image intensified array. Aircraft operational attributes of quick reaction capability and ready availability when satellite coverage is not available were found to be complementary to the secure and covert coverage of satellite sensors. Aircraft may use laser sensors in addition to passive sensors and thereby make possible range gating for depth measurement and new interactions such as fluorescence and Raman and Brillouin scattering which offer non-site specific and simpler data interpretation algorithms.

14. SUBJECT TERMS	15. NUMBER OF PAGES
satellite multispectral imaging, ocean optics, chlorophyll airborne lidar, Raman, Brillouin	97
	. PRICE CODE

17. SECURITY CLASSIFICATION OF REPORT	18. SECURITY CLASSIFICATION OF THIS PAGE	19. SECURITY CLASSIFICATION OF ABSTRACT	20. LIMITATION OF ABSTRACT
UNCLASSIFIED	UNCLASSIFIED	UNCLASSIFIED	

FOREWARD

This report was prepared by EOO, Inc. Sunnyvale, California under Office of Naval Research (ONR) Contract N00014-93-C-0155 and describes work conducted by EOO, Inc. from April 1993 through June 1995 in support of the coastal water predictive model development program The cognizant technical personnel for ONR have been Dr. William Stachnik and Dr. David Johnson. Mr. Donald Leonard was the Principal Investigator during the entire course of the contract. Mr. Leonard was assisted by Dr. Thomas Driscoll and Dr. Paul Titterton.

The cooperation and time made available for discussion of technical issues by the following persons is gratefully acknowledged:

- Dr. Frank Hoge, NASA Wallops Flight Center; for information concerning the airborne oceanographic lidar (AOL) data collection and analysis
- Dr. Chuck McClain, NASA Goddard; for SeaWiFS performance details
- Dr. John Barker, NASA Goddard; for information concerning LANDSAT limiting noise sources when operating over coastal water bodies
- Dr. Joan Cleveland, CHORS; for information concerning the optical properties of chlorophyll
- Dr. Jon Schoonmaker, NCCOSC; for information concerning in situ instrumentation for measurement of water optical properties
- Mr. Chris Simi, NVEOL; for information concerning multispectral optical imaging test data from Shuttle missions.

Special recognition and acknowledgment is given to Dr. Jack McKay of RSI, Inc. for collaborating with EOO, Inc. in the concept definition of a dedicated satellite sensor for multispectral imaging of upwelling solar radiation in coastal zone water. We also wish to acknowledge the close cooperation of Mr. Robert Hammond of SAIC, the principal investigator for coastal water clarity predictive model development, which this program supported.

A listing of the principal meetings and workshops which EOO, Inc. initiated and/or participated in during the course of this work are listed in Appendix A.

TABLE OF CONTENTS

LIST OF FIGURES

LIST OF TABLES

1.0 Executive Summary

This report is concerned with the problem of making environmental measurements to provide data for the prediction of the optical properties of coastal waters. This executive summary is organized to provide the highlights and salient points of each of the major sections of the report, which are separately presented in this summary.

A major result of the work was the development of a satellite concept definition that can provide measurements of coastal zone water properties with both the necessary sensitivity and spatial resolution. Existing satellites, both operational and those planned for launch, have either the requisite sensitivity or the requisite spatial resolution, but not both in combination.

Section 2.0 Introduction

- The goal of this contract was to evaluate remote sensing concepts and other potential solutions to the problem of providing initial conditions for the Coastal Water Clarity (CWC) predictive model development program. EOO worked closely with SAIC, the CWC model development contractor, with the division of responsibility depicted in Figure 1-1

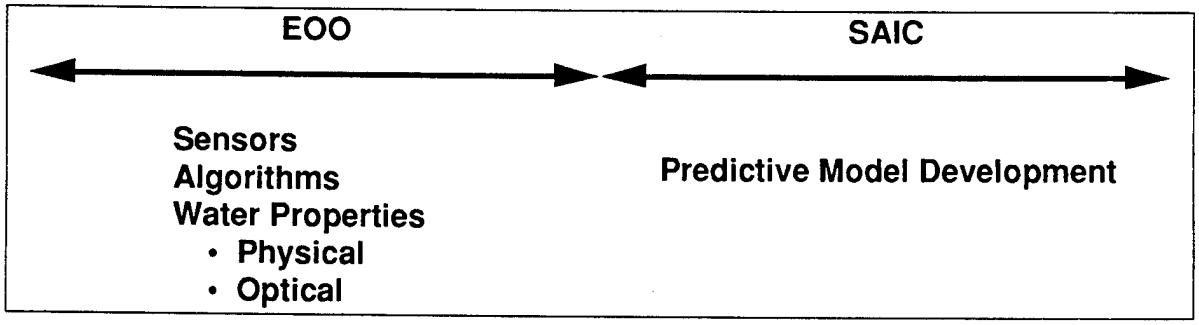

Figure 1-1 Program Responsibilities of EOO and SAIC

- A major portion of the work was directed to survey the existing remote sensing capability, especially satellite borne systems, to see if the initial conditions for the CWC model can be met with existing reconnaissance technology.
- Emphasis is on quantitative, optical remote sensing of water physical and optical properties.
- Objective is to define operational reconnaissance system concept and also define a road map to develop such a system.

Section 3.0 Statement of the Problem

- The Navy's current warfighting strategy places increasing emphasis on naval operations in the coastal water zone. Many Navy warfighting systems are critically dependent on the intrinsic optical properties of the subsurface water.
- Predictive models of optical properties for coastal water do not currently exist, or are in their early stages of development.
- Operational reconnaissance systems have not yet been defined that can determine optical properties on a timely basis, or that can measure water conditions for the initialization of the predictive models now under development.
- The identification of a suitable reconnaissance system should have emphasis on existing systems and off-the-shelf equipment and technology, so as to involve the minimum of development efforts.

Section 4.0 General Review of Possible Measurement Methods

- Initial effort consisted of a collaborative effort with SAIC to provide an overall requirements definition of the coastal water physical and optical properties that are required as inputs for initialization and updating of a predictive model.
- The required spatial resolution in the coastal zone was in the 10 to 30 m range.
- The following were deemed to be the minimum remote sensing requirements for the water physical and optical properties for predictive model initialization and updating.
- The accuracy requirements are application specific and need to be examined for specific operational systems. This was not done during the program

Table 1-1 Water Physical Properties Requirements

Parameter	Symbol (units)	Range or Domain	Accuracy
Chlorophyll Concentration	ch [mg/m^3 ($\mu g/l$)]	$0.5 \leq ch \leq 50$ [Depth: 0 to 5 KD]	TBD
Sediment Concentration	sed (mg/l)	$1 \leq sed \leq 200$ [Depth: 0 to 5 KD]	TBD
Dissolved Organic Material	DOM (m^{-1} @ 440 nm)	$0.1 \leq DOM \leq 0.5$ [Depth: 0 to 5 KD]	TBD

Table 1-2 Coastal Water Optical Properties Requirements

Parameter	Symbol (units)	Range or Domain	Accuracy
Diffuse Attenuation Coefficient	K (m^{-1})	$0.05 \leq K \leq 0.25$ [$430 \leq \lambda \leq 600$ nm, Depth: 0 to 5 KD]	TBD
Beam Attenuation Coefficient	c (m^{-1})	$0.07 \leq c \leq 0.3$ [$430 \leq \lambda \leq 600$ nm, Depth: 0 to 5 KD]	TBD
Backscatter Coefficient	b_b (m^{-1} $srad^{-1}$)	$0.0005 \leq b \leq 0.01$ [$430 \leq \lambda \leq 600$ nm, Depth: 0 to 5 KD]	TBD

- The reconnaissance system trade space included the following principal ingredients: (1) satellite-borne, scanning, multi-spectral radiometers; (2) airborne multi-spectral, imaging radiometers; (3) airborne, depth-resolving lidar; and (4) underwater autonomous vehicle (AUV) borne optical sensors.
- Satellites provide worldwide coverage in a secure and covert manner and would be cost effective if existing satellites, sensors and data interpretation techniques could be used. The physics of the satellite measurement is limited to passive measurement of sunlight induced upwelling spectra.
- Aircraft can provide quick reaction and ready availability in particular when satellite coverage is not available due to either orbit constraints, cloud cover or lack of sufficient daylight. Aircraft may use active laser illuminated sensors in addition to passive techniques and can thus provide day and night coverage and measurements as a function of depth using pulsed lasers.
- In situ point sampling may sometimes be necessary either for calibration of an operational system; for ground truth measurement of intrinsic properties in a validation test; or because no other method can provide the required data.

Section 5.0 Quantitative Optical Remote Sensing

5.1 Satellite-borne scanning multi-spectral radiometers for coastal water optical properties predictive model initialization and update.

- Quantitative data and graphs are shown for existing and planned satellite platforms that relate satellite sensor sensitivity, water-leaving radiance, atmospheric path radiance and pixel size on the ocean surface.
- All existing or planned satellite imaging sensors cannot meet the coastal zone combined requirement of small pixel size (10 to 30 m) and high sensitivity(≤ 0.1 W / m^2-μm-sr). Figure 1-2 summarizes this on a plot of sensitivity

(noise equivalent radiance) as a function of pixel size. The desired operating region is indicated in the lower left of the chart, which meets or exceeds the sensitivity of a SeaWiFS and the spatial resolution of a LANDSAT.

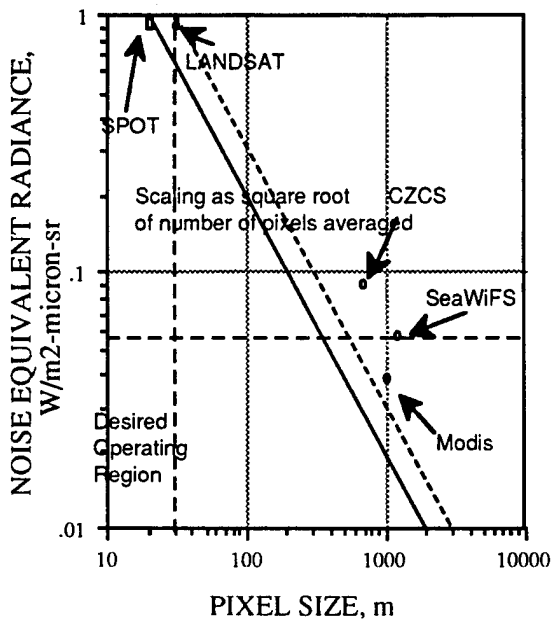

Figure 1-2 Satellite Sensitivity vs. Pixel Size

- Satellites designed for ocean sensing have adequate sensitivity, i.e., better than 0.1 W / m^2-μm-sr, but have a pixel size ≈ 1 km that is too large for coastal zone utilization.
- Satellites designed for land sensing typically have the appropriate pixel size, i.e. 20 to 30 m, but have a sensitivity ≈ 1 W / m^2-μm-sr that is too coarse.
- Since atmospheric path radiance comprises ≈90 percent of the radiance received at the satellite, proper path radiance correction is critical for adequate measurement of the water leaving-radiance and the correct retrieval of water properties.
- Using a pixel averaging technique, a LANDSAT image was analyzed to test published retrieval algorithms, generate contour maps of water physical properties for initialization of the predictive model, and establish the processing procedures to be used on future studies.

5.2 In addition to high spatial resolution muti-spectral imagery, the unique contribution that aircraft sensors provide (that is not available with satellite sensors) is the ability to use an active laser illuminated system.

- A laser airborne fluorosensor can provide accurate fluorophore concentration measurements by normalizing the fluorescence signal with the concurrent water Raman signal.
- A pulsed laser Brillouin sensor, can obtain the vertical profile of the logarithm of the downwelling irradiance, and thus obtain a direct measure of the diffuse attenuation coefficient.
- A pulsed lidar, measuring both Raman and on-frequency components can determine the backscatter coefficient as a function of depth.

Section 6.0 Remote Sensing Development

- Two options for improved multi-spectral imaging were selected and developed as concepts that could improve the capability of satellite remote sensing of coastal zone water and enable the requisite sensitivity and spatial resolution.
- One concept uses a narrow swath sensor array with longer effective dwell time achieved by time-delayed integration (TDI). This concept is illustrated in Figure 1-3

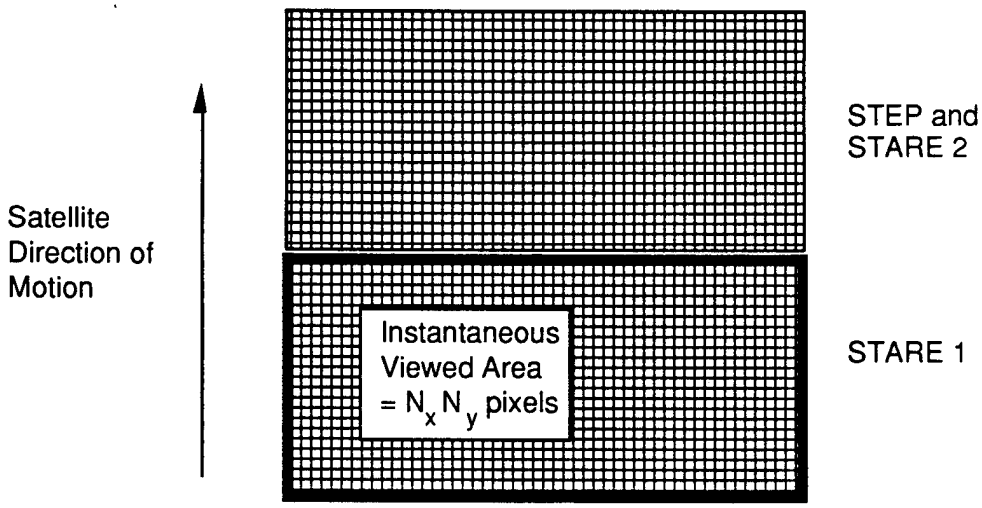

Figure 1-3 Concept for Longer Effective Dwell Time Satellite Sensor Array

- The second concept utilizes a shot-noise limited image intensified array sensor, and the device currently commercially marketed by Xybion is analyzed as an example.

Section 7.0 Conclusions and Recommendations

- A requirements definition is required that would present a matrix of critical optical properties, with range and accuracy, vs. operational optics-oriented Navy systems.
- An operations concept is required that would include combined usage, data fusion and interfaces with Navy users.
- Operational reconnaissance system development should emphasize the following:
  (1) Satellite - optimal exploitation of existing and planned sensor systems and exploratory development of narrow-swath, small pixel, high SNR add-on concepts;
  (2) Aircraft - exploratory development of unmanned systems with emphasis on both passive and active sensors and fusion algorithms; (3) In situ - baseline concepts strongly dependent on operational concept.
- Validation tests of sensors and algorithms should be planned to define and resolve critical issues. A candidate airborne passive/active measurement platform (the NASA Wallops Airborne Oceanographic Lidar) was selected for test use in conjunction with satellite overflights and in situ measurements.
- A reconnaissance system implementation plan should include the optimum exploitation of existing and planned capabilities, as well as the development of unique and necessary new capabilities.

2.0 Introduction

This report describes the work performed and the results obtained under Office of Naval Research Contract N00014-93-C-0155, "Coastal Water Optical Properties Prediction Development" during the period June 1993 to December 1994.

The goal of Contract N00014-93-C-0155 was to evaluate remote sensing concepts and other potential solutions to the problem of providing initial conditions for the Coastal Water Clarity (CWC) predictive model development program. During the contract period, EOO, Inc. has worked closely with the model development contractor (SAIC), through a series of meetings and workshops, to define requirements for the water property initial conditions. The division of responsibility is depicted in Figure 2-1.

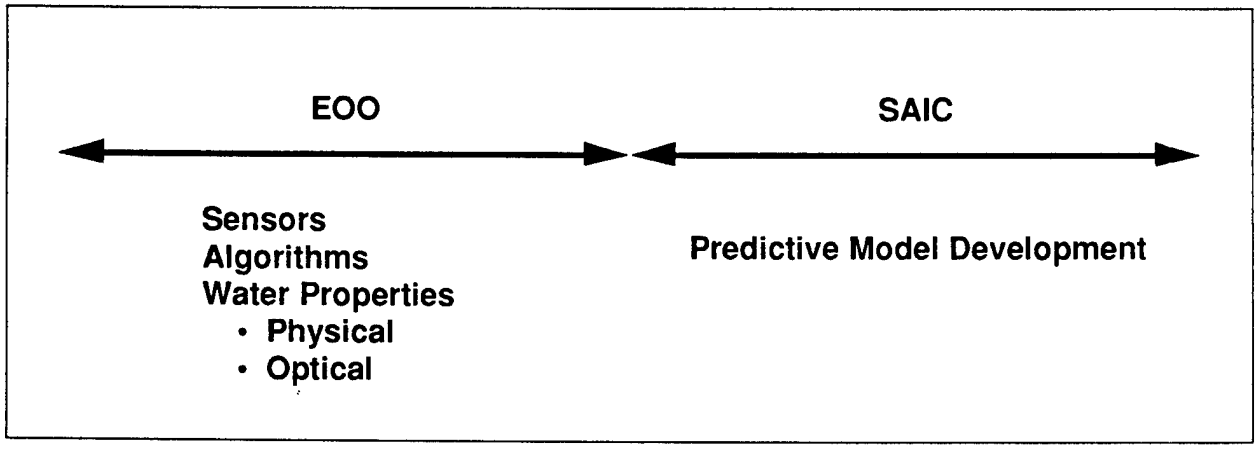

Figure 2-1 Program Responsibilities of EOO and SAIC

In the model being developed, these initial water properties then evolve in time as the CWC predictive model is time stepped. The future state of the optical properties is then inferred by means of an optics model from the predicted water properties. The most important water properties that strongly influence optical properties are the concentrations of chlorophyll, sediment and dissolved organic manner.

The volume scattering function (VSF), the absorption coefficient, and the fluorescence and Raman excitation/emission spectral cross-sections are the fundamental inherent optical properties from which all other apparent properties can be derived. It is the determination of these inherent properties as a function of lateral position and depth that is the basic goal of the optical properties prediction development work. However, it is possible in some instances that the measurement of an apparent property may be accomplished relatively easily and would provide exactly the information needed to predict the performance of a Navy optical system. An example is

the determination of diffuse attenuation from depth resolved airborne lidar data for determining the performance of bathymetry, anti-submarine or anti-mine, or laser communications systems.

The water properties and the critical optical properties are measured both for the purpose of providing initial conditions for the predictive model, and for use in validation of the time evolution results of the predictive model. The measurements are needed both during the development phase of the model and for successful utilization of the model when it becomes an operational tool. The specific instruments and their platforms could of course be entirely different during model development and operational use.

A major portion of this work has been to survey the existing remote sensing capability, especially satellite borne systems, to determine if the initial conditions can be measured/inferred by existing satellite sensors. The results of this work showed that existing satellites are either designed for land operations (i.e. LANDSAT) or open ocean observations (i.e. SeaWiFS), and that neither class of satellite satisfies the specific requirements for coastal water measurements. The LANDSAT pixels are the right size but the sensitivity is too low, whereas SeaWiFS has adequate sensitivity but the pixels are too large.

In addition both SeaWiFS and LANDSAT have severe problems when operated across a bright "edge" such as a coastline. SeaWiFS has the problem of unacceptable internal light scattering for the first 7 or 8 rows of water pixels (7 or 8 km) when used along a beach or other bright land mass. LANDSAT exhibits a loss of sensitivity when the scanner sweeps from the coastline onto the water mass. EOO, Inc. has expended considerable effort to extract as much information as possible from degraded LANDSAT coastline images. The analysis of two LANDSAT images of the California coast has been used in direct support of the SAIC effort.

Sensor concepts for satellite usage that are optimized for coastal water measurements have been developed. These concepts considered trades which included dwell time vs. swath width, and shot noise limited sensors with gain vs. internal noise limited devices. In principle a satellite sensor could be optimized for coastal zone measurements, although we know of no present plans to develop such a system.

The work also investigated the state-of-the-art of retrieval algorithms for extracting the optical properties and the water properties from passive radiometric spectral data. We have concluded that the situation with respect to Case II water (i.e. water which

simultaneously contains a multiplicity of components) is in a state of flux and that large errors are possible in estimating the retrieved water properties even with accurate remotely sensed passive data. There is a strong indication that an active system (using laser illumination) would be more accurate, and also achieve a measure of depth resolution. Such an active system would require an aircraft platform to achieve even moderate area coverage rates. Although the emphasis has been on remote sensing, in-situ devices were also investigated, especially electro-optical sensors that could best be adapted to autonomous operation.

In addition to investigating sensors and methods for providing initial conditions and upgrades to an operational predictive system, the effort also considered field test instrumentation that would be useful for model validation.

3.0 Statement of the Problem

Numerous war fighting systems are available, becoming available, or have been shown to be feasible for Navy tactical use in coastal water applications that are critically dependent on the optical properties of subsurface water. These systems include those listed in Table 3-1.

Table 3-1 Navy Warfighting Systems Dependent on Subsurface Optical Properties

• Imaging Optical Radar of Submerged Targets
- Anti-Mine Warfare
- Anti-Submarine Warfare
• Passive Optical Surveillance Systems for Submerged Targets
- Ship or Aircraft Platform
- Submersible Systems (AUV or SEALS)
• Bathymetry
• Tactical Oceanography (lidar measurement of temperature, salinity and sound velocity profiles)
• Laser Communication Links with Underwater Platforms

Each of these systems will be developed and deployed, only as it significantly enhances the Navy's war fighting effectiveness. However, in general it is not at present possible to accurately predict the performance of these systems at any particular location and at any specific time unless certain critical optical properties of the water are known. These optical properties are identified in the performance models for each system, and typically include those listed in Table 3-2. These optical properties include some apparent optical properties that should be distinguished from fundamental intrinsic optical properties which include the absorption coefficient, the volume scattering function and fluorescence cross-sections. The apparent properties can be derived from the intrinsic properties, but the reverse is in general not true.

From first principles it is therefore desirable to determine the intrinsic properties, from which any other optical property of interest can be calculated. These inherent properties can either be derived either from a knowledge of the water physical properties, or from direct measurement of the inherent optical properties themselves. In some instances an apparent optical property that is a key determinant of the performance of an optical warfighting system, can be either measured directly or derived directly from a water physical property. In such cases an expedient procedure

would be to utilize the apparent property directly, and not attempt to determine the inherent optical properties.

Table 3-2 Critical Optical Properties for Performance Models

K	=	Diffuse Attenuation Coefficient, m^{-1}
c	=	Beam Attenuation Coefficient, m^{-1}
b_b	=	Backscatter Coefficient, $m^{-1}sr^{-1}$
PSF	=	Point Spread Function

3.1 Overall Problem Statement

The approaches to determining the critical optical properties for a given Navy tactical situation are: (1) use historical data bases; (2) use timely reconnaissance measurements and their interpretation for the area in question; or (3) use a combination of (1) and (2), with a predictive model

The third approach, that of using a predictive model in combination with historical data bases and timely initial conditions derived from reconnaissance information, was the primary problem addressed in the work reported herein.

The current problem is threefold:

(1) Predictive models of optical properties do not currently exist, or are in their early stages of development, and will be difficult to generalize and validate.
(2) Operational reconnaissance systems (to determine optical properties on a timely basis or to measure initial conditions suitable for the predictive models now under development) have not yet been defined.
(3) Historical data bases for many locations of potential interest are not available.

The architecture that needs to be developed is shown in Figure 3-1, which depicts a reconnaissance system being used to provide input to the operational military decision making process. The reconnaissance system provides this information in three different ways; (1) directly as a stand alone system for providing the optical properties as real-time input to the decision making process; (2) by providing initial conditions and updates of both optical properties and water physical properties (i.e. chlorophyll, sediment and dissolved organic material (DOM) concentrations) to a predictive model; and (3) as a source of archival data which is used at some subsequent time, either directly in the decision making process or as additional input to the predictive model.

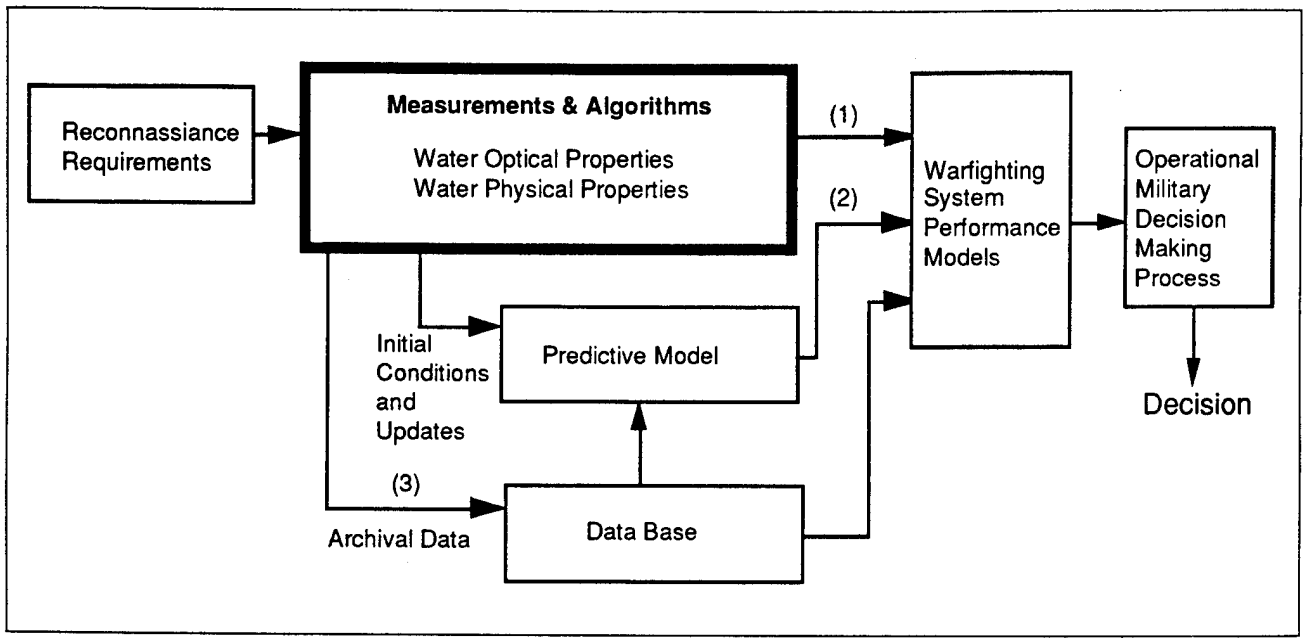

Figure 3-1 Coastal Water Optical Reconnaissance System Architecture

The present work addressed the part of the reconnaissance system that is contained in the box labeled "Measurements and Algorithms". The key issue is the selection of the appropriate sensor and sensor platform, given the reconnaissance requirements for a given mission. The choice of platform was broken down into remote sensing satellite and aircraft platforms and in situ. platforms. Electro-optical sensors were emphasized because they encompass virtually all the sensors that have utility for measurement of the relevant water properties and uniquely define those sensors that can directly measure water optical properties. Another major issue is the selection of the appropriate data retrieval algorithm to convert the sensor signals into water physical and optical properties.

4.0 General Review of Possible Measurement Methods

This section gives a general review of potential measurement methods that have been considered for a reconnaissance system to determine the physical and optical properties of coastal water regions. The initial effort consisted of a collaborative effort with SAIC to provide an overall requirements definition of the physical and optical properties that are required as inputs for initialization and updating of the predictive model. The flow of these remote sensing derived inputs into the predictive model and their subsequent utilization by the model is shown in Figure 4-1. The vertical dashed line separates the flow diagram into the SAIC portion which is the model development activity and the EOO portion which is reconnaissance system development activity.

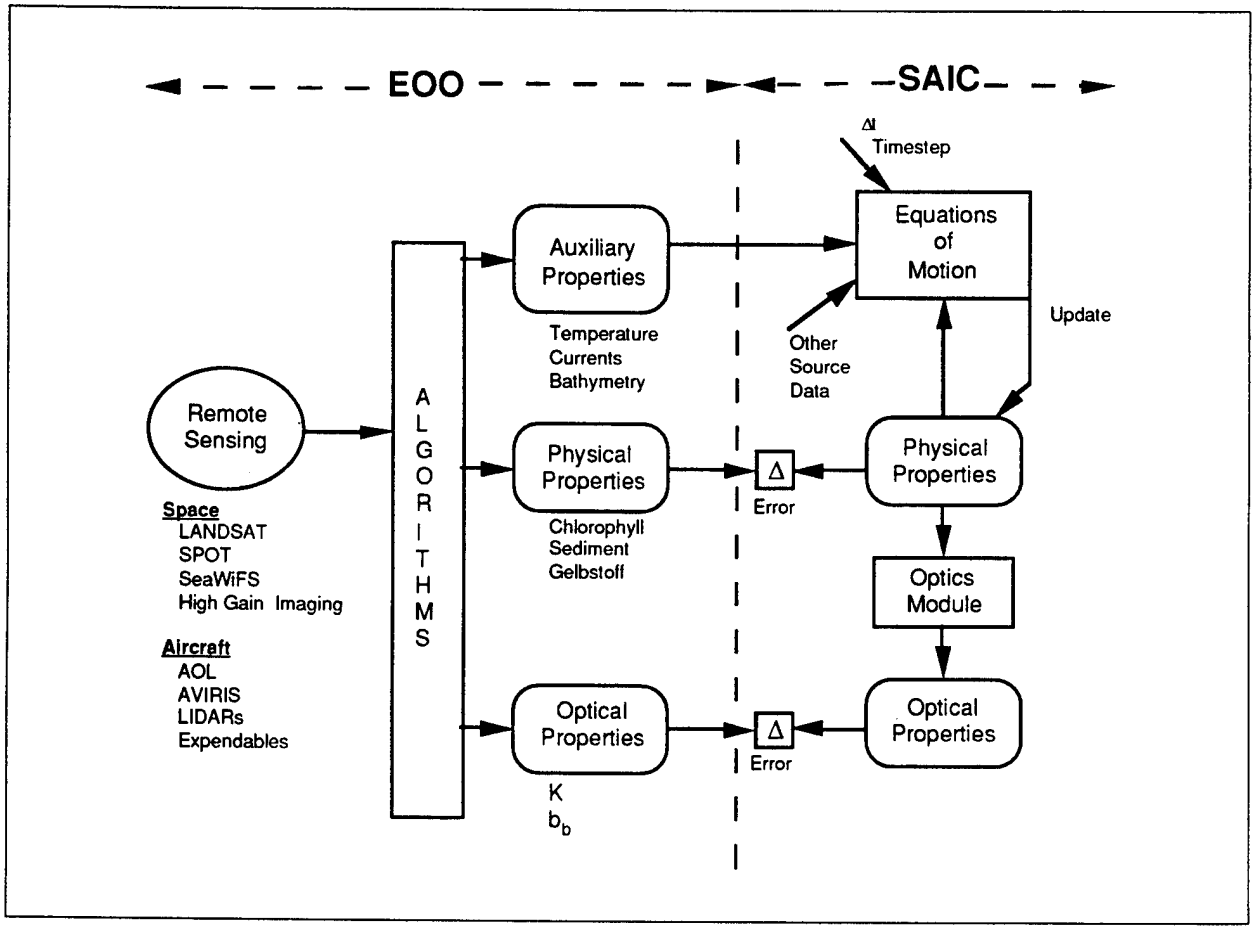

Figure 4-1 Coastal Water Clarity Reconnaissance Flow Diagram

The predictive model is based on equations of motion that define the physical properties of the coastal water region as functions of time. Through appropriate time-step evolution the model predicts the physical properties of the coastal water region at some future time. At any step in the process an optics model is used to determine the optical properties of the water from the physical properties then current. The

reconnaissance system is intended to provide inputs to the predictive model of the values of the water physical properties and some auxiliary properties for initialization and also for possible periodic updates and corrections. The reconnaissance system also is intended to provide a measure of some of the key optical properties as a self consistency check on the validity of values of the optical properties being determined by the optics module from the physical properties within the model.

In collaboration with SAIC, estimates were made of the range of values and the accuracy required for some of the water physical and optical properties that were required by the predictive model as described above. The water optical properties requirements are summarized in Table 4-1. The water physical properties requirements are summarized in Table 4-2. It should be noted that the accuracy requirements are application specific and need to be examined for each operational system. This was not done during the program

Table 4-1 Coastal Water Optical Properties Requirements

Parameter	Symbol (units)	Range or Domain	Accuracy
Diffuse Attenuation Coefficient	K (m^{-1})	$0.05 \leq K \leq 0.25$ [$430 \leq \lambda \leq 600$ nm, Depth: 0 to 5 KD]	TBD
Beam Attenuation Coefficient	c (m^{-1})	$0.07 \leq c \leq 0.3$ [$430 \leq \lambda \leq 600$ nm, Depth: 0 to 5 KD]	TBD
Backscatter Coefficient	b_b (m^{-1} $srad^{-1}$)	$0.0005x \leq b \leq 0.01$ [$430 \leq \lambda \leq 600$ nm, Depth: 0 to 5 KD]	TBD

Table 4-2 Coastal Water Physical Properties Requirements

Parameter	Symbol (units)	Range or Domain	Accuracy
Chlorophyll Concentration	ch [mg/m^3 (µg/l)]	$0.5 \leq ch \leq 50$ [Depth: 0 to 5 KD]	TBD
Sediment Concentration	sed (mg/l)	$1 \leq sed \leq 200$ [Depth: 0 to 5 KD]	TBD
Dissolved Organic Material	DOM (m^{-1} @ 440 nm)	$0.1 \leq DOM \leq 0.5$ [Depth: 0 to 5 KD]	TBD

The trade space that must be considered for the reconnaissance system is shown in Figure 4-2. The specific war fighting system application will determine the

reconnaissance system output requirements, which in turn will determine the appropriate sensors and algorithms that need to be used.

The primary intent of the work reported is not to advance the state of the art of remote sensing but rather to provide a compilation and critique of existing sensors and to make recommendations for their utilization for specific missions. A secondary intent of the work is to make recommendations for development of new reconnaissance systems and sensors in order to provide critical capabilities that do not now exist.

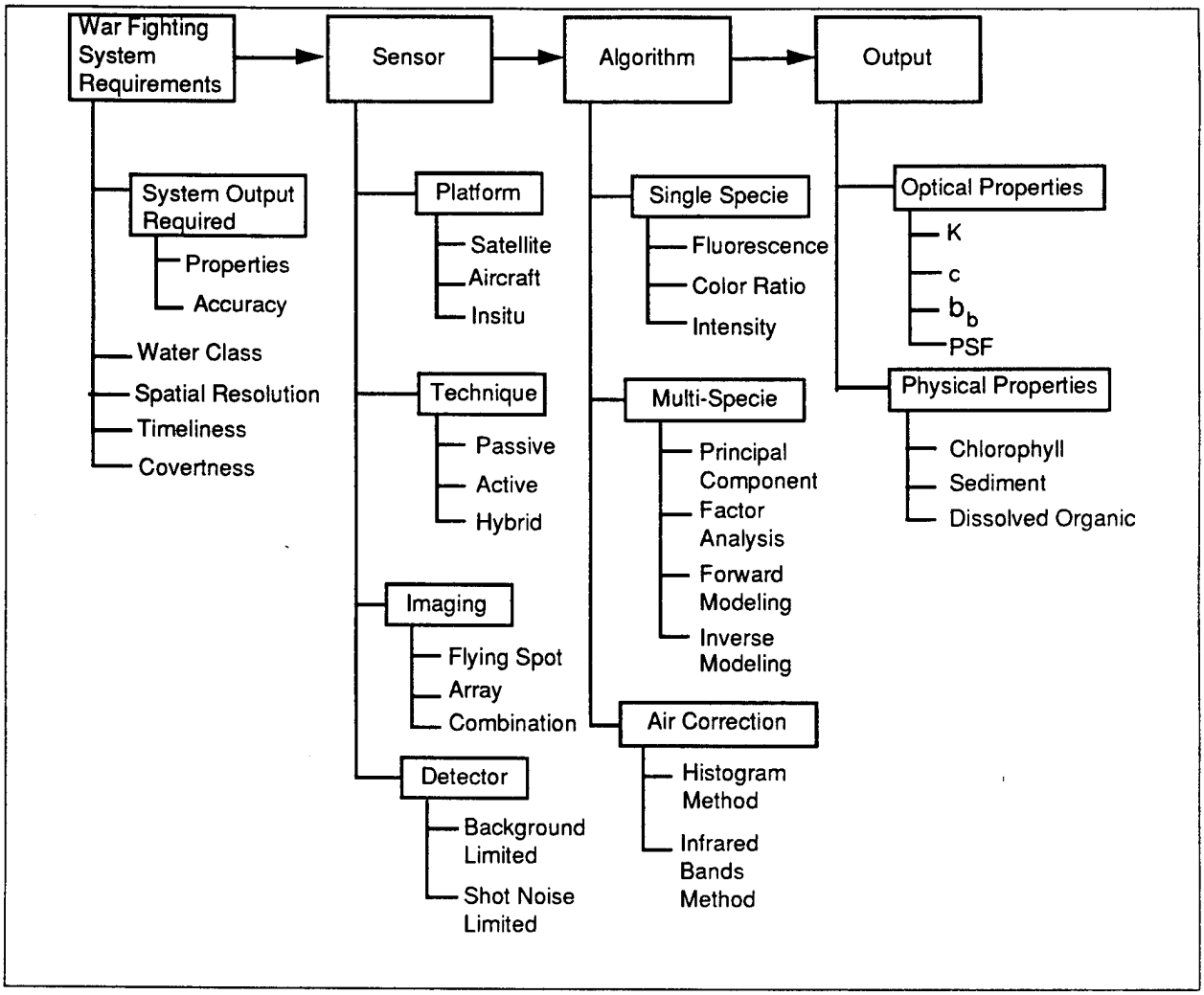

Figure 4-2 Trade Space of the Reconnaissance System

As shown in Figure 4-2, the measurement methods break down into remote sensing methods which enable coverage of a large grid (many square kilometers) on a synoptic time scale, and in situ methods, which are essentially point measurements. Although remote sensing is in general desired, in situ point sampling may sometimes be necessary either for calibration of an operational system; for ground truth measurement

of intrinsic properties in a validation experiment; or because no other method can provide the required data.

The performance of readily available instrumentation that can be used to satisfy the model input requirements was assessed. This assessment used the following generic set of instrumentation as a baseline.

- Satellite-borne scanning, multi-spectral radiometers of the CZCS type, and other satellite data such as available from weather satellites;
- Airborne multi-spectral radiometers, equivalent to the satellite-borne CZCS, but with the capability for a much smaller horizontal pixel size;
- Airborne lidar, capable of probing the ocean down to KD values of ≈ 5. This includes both conventional lidar and the EOO-patented techniques of detection of Brillouin scattering for temperature, K and b_b;
- In situ equipment, carried by an autonomous underwater vehicle (AUV), and capable of measuring the inherent optical properties;
- Auxiliary equipment for measuring local temperature, optical and other water properties, as needed to provide ground truth and data base information.

In this study we have concentrated our efforts on optical remote sensing systems that can be employed on either satellite or aircraft platforms. This emphasis resulted from the requirement for large area coverage and operational considerations. The optical remote sensors can be further subdivided into passive or active, imaging or non-imaging, and multi-spectral or monochromatic systems. The aircraft active systems also have the capability for depth resolved measurements. Evaluation has been restricted to several specific platforms and systems, both satellite and aircraft, that are either being developed or are already well established tools. The hierarchy of the remote sensing systems evaluated in the this study is shown in Figure 4-3. The potential advantages of data fusion from different optical remote sensors, e.g. satellite/passive and aircraft/active has also been considered.

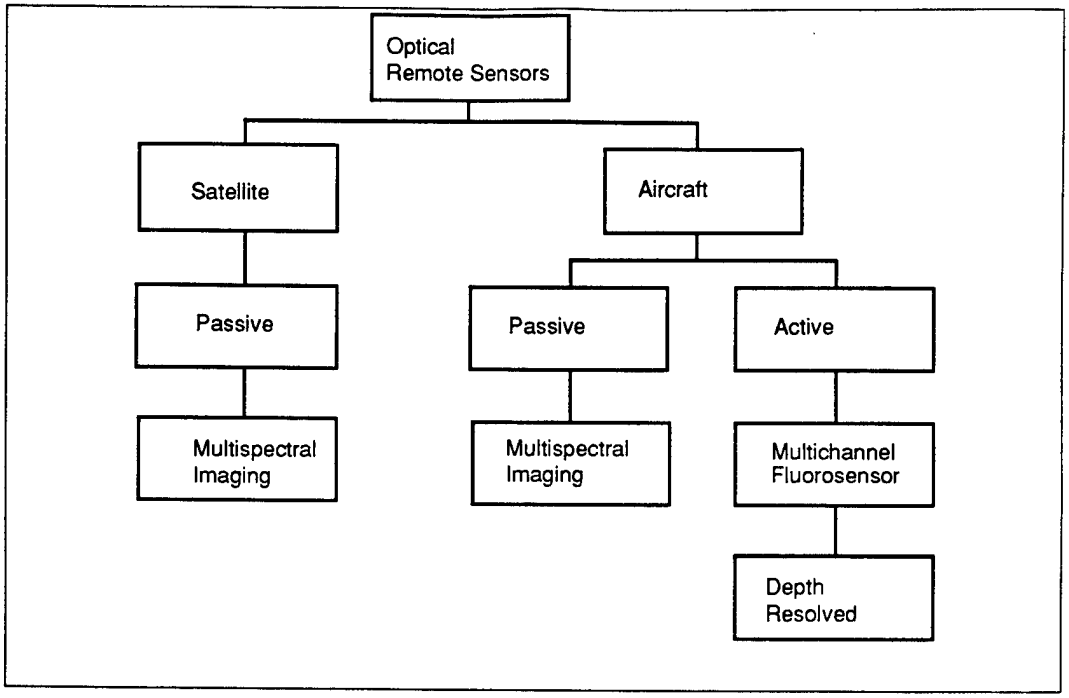

Figure 4-3 Hierarchy of Remote Sensing Systems

The satellite and aircraft measurement methods are quite different and each has unique attributes that the other does not. These attributes can be classified as operational and technical and are summarized in the following.

The operational attributes of satellites are primarily that of worldwide coverage in a secure and covert manner. The satellite measurement is also very cost effective, if existing satellites, sensors and data interpretation techniques can be utilized. The aircraft operational attributes are that of quick reaction capability, ready availability in particular when satellite coverage is not available, due to either orbit constraints, cloud cover, or lack of sufficient daylight. The aircraft also has the advantage that active systems can be utilized during day or night and can provide information as a function of depth.

The technical attributes of the satellite measurement is such that the physics of the measurement is limited to sunlight reflection phenomena. Aircraft may use active sensors in addition to passive sensors, and thereby bring to bear the different physics of active systems including range gating for depth measurement and specific scattering interactions such as fluorescence, Brillouin and Raman processes which in many cases have much simpler and non-site specific data interpretation algorithms.

In addition to the actual sensor and signal extraction hardware, of comparable importance is the choice of algorithm utilized to convert the raw sensed data into useful information concerning the physical and optical properties of the coastal water. For some sensing methods, such as the aircraft active lidar sensing of chlorophyll, the specificity of the method is such that the algorithms are very simple and the reliability is very great. For other sensing methods, such as satellite multispectral imaging, the algorithms may become very complex and the reliability becomes low, especially in Case II coastal water in which there is a mixture of chlorophyll and other pigments, sediment and dissolved organic matter where each component contributes significantly to the resultant optical properties.

The following subsections describe in more detail the various elements of the trade space shown in Figures 4-2 and 4-3.

4.1 Satellite Remote Sensing Measurements

Satellite-borne sensors measure only radiance at the satellite, but the water property retrieval algorithms depend on the water-leaving radiance. The radiance at the satellite is mostly (≈ 90%) atmospheric path radiance caused by sunlight scattered from atmospheric aerosols and molecules. Correction algorithms to account for sky radiance must be first applied before the water-leaving radiance is processed to determine water properties. Other error sources in calculating water-leaving radiance arise from sun glitter on the water and sky reflection from the water. These can be minimized by satellite orientation or averaging.

The open literature, product brochures, and planning documents were reviewed to compile the necessary data. The spectral coverage of existing and planned satellite sensors is shown in Figures 4-4 and 4-5, respectively. The relevance of the various spectral coverages to the ocean properties retrieval problem will be discussed in Section 5.

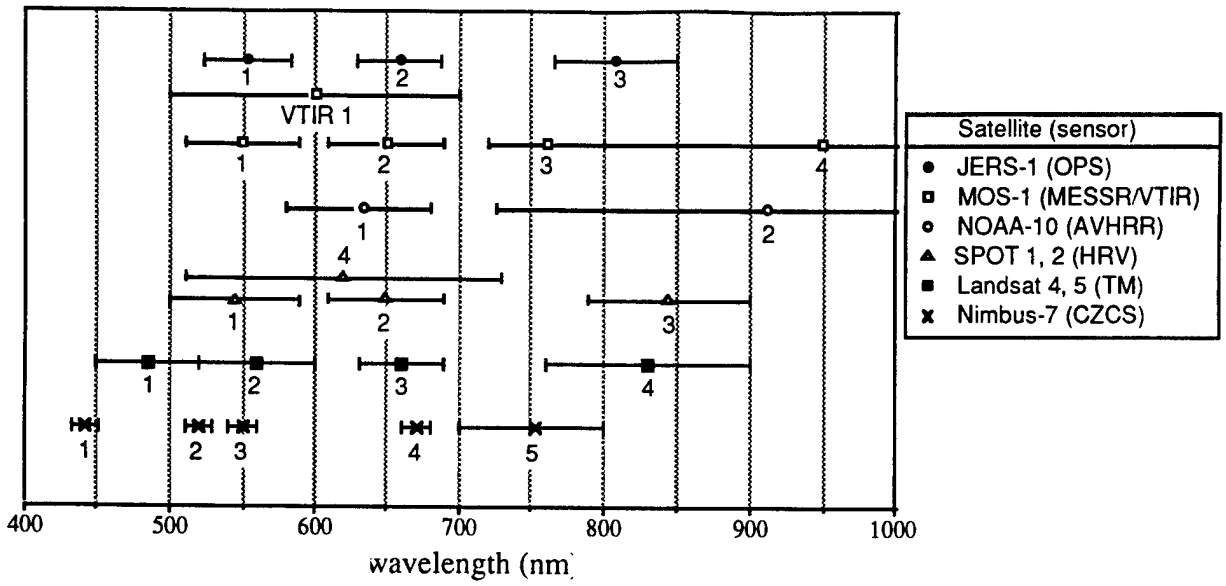

Figure 4-4 Wavelength coverage of Existing and Past Satellite Sensors

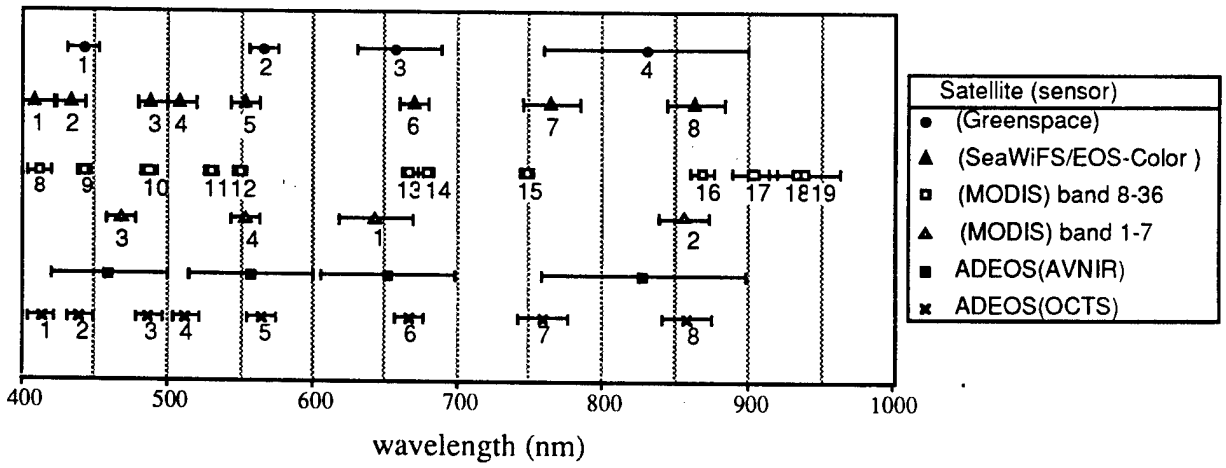

Figure 4-5 Wavelength Coverage of Planned Satellite Sensors

The sensitivity of the satellite sensor is an important element of suitability, both in terms of signal to noise ratio (SNR) and noise equivalent radiance. The ocean has low reflectivity, in general, compared to the adjacent land, and the atmospheric path radiance is roughly 90% of the total observed radiance. A high SNR is needed to see the dim water against these bright sources. The noise equivalent radiance of selected satellite sensors, both existing and planned, is shown in Figure 4-6. These values were found in the open literature, product brochures and planning documents, as listed in the references.

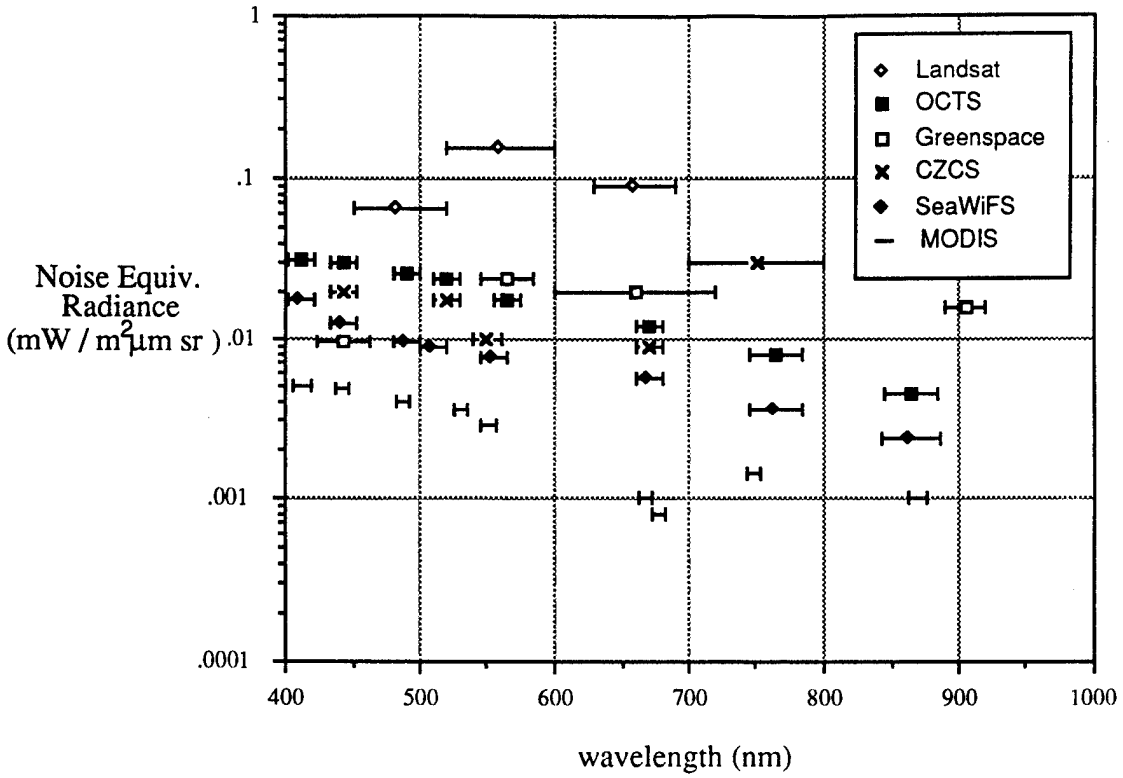

Figure 4-6 Satellite Sensor Sensitivities vs. Wavelength

Coastal features have a 10 to 30 m scale size, and the predictive model uses a 100 m grid, so the satellite sensor should have at least 10 m resolution. In open ocean, the water is featureless on a much larger scale size, so satellite sensors with a larger pixel size have utility. Ocean color data from sensors with large pixel sizes may give boundary values for the coastal zone predictive model.

The predictive model needs updates periodically from remote sensors to correct errors in calculated ocean physical properties. The satellite coverage rate is an important parameter in determining its utility. In general, the satellite sensors with high spatial resolution have a larger revisit time since the total number of detectors, and swath width are limited. We have compiled a table of pixel size and swath width (which roughly indicates the revisit time) for selected satellite sensors, both existing and planned.

The data for pixel size and swath width shown in Table 4-3 was found in the open literature, product brochures and other documents as seen in the references.

Table 4-3 Satellite Sensor Pixel Size and Swath Width (Revisit Time)

Satellite (sensor)	pixel size (m)	Swath width (km)	approx. revisit time (days)
JERS-1 (OPS)	18 x 24	75	
MOS-1 (MESSR/VTIR)	50/900	100	17
NOAA-10 (AVHRR)	1100-4000		8
SPOT-1, -2 (HRV)	20/10	60	26 (2-3)
LANDSAT 4,5 (TM)	30	185	16
Nimbus 7 (CZCS)	825	1600	
(Greenspace)	300	1225	1-2
Seastar (SeaWiFS)	1100	2801	1-2
(MODIS b 8-36)	1000	2330	1-2
(MODIS b 3-7)	500		
(MODIS b 1-2)	250		
ADEOS (OCTS)	700	1400	few
ADEOS (AVNIR)	16	80	

Source materials from which the data in Table 4-3 was derived.

[1] M.D. Thompson, J.F.R. Gower, and H.H. Zwick, "Medium Resolution Satellite Sensing for Coastal Zone Monitoring: A Canadian West Coast Example", 1st Thematic Conf. on Remote Sensing of Marine and Coastal Environment, New Orleans, 1992 pg. 971.
[2] T. Iida, and Y. Sasano, Research Announcement, Advanced Earth Observing Satellite (ADEOS) Cal/Val and Science #JRA-93-001.
[3] Earth Observation Satellite Co., Lanham, MD
[4] MODIS Technical Specifications, Hughes, Santa Barbara Research Center, Goleta, CA.
[5] V.V. Salamonson, "Earth Observations through the Earth Observing System (EOS)/ Moderate Resolution Imaging Spectroradiometer (MODIS) Multispectral Capability and Combined Observations with other EOS Instruments", ISP conference paper 4.
[6] S.B. Hooker, W.E. Esaias, G.C. Feldman, W.N. Gregg, and C.R. McClain, "An Overview of SeaWiFS and Ocean Color", NASA Technical Memorandum 104566, v1, 1992.
[7] SPOT User's Handbook, rev. 2 (June 1991), SPOT Image Corporation, Reston, VA, 22091.

4.2 Aircraft Remote Sensing - Passive Systems

Aircraft systems operate at much lower altitudes than satellite systems, and therefore can have much greater collection efficiency. This has enabled aircraft systems to measure much smaller pixel sizes with higher sensitivity. Also, such systems have been operated with greater numbers of spectral channels than have been achieved in operational satellite systems - in part because of the difficulty (and therefore cost) of high bandwidth data collection from satellites.

A major step in multispectral imaging (also known as imaging spectrometry) was the NASA development of the Airborne Visible Infrared Imaging Spectrometer (AVIRIS) [Carder, 1993]. Operational in 1987 it is still in current use on the NASA ER-2 and is

continually being re-engineered and upgraded. AVIRIS operates at an altitude of 20 km with a spatial resolution of 20 m over a swath of 11 km. The spectral resolution is 10 nm with 224 contiguous bands in the spectral region of 0.4 to 2.5 μm.

A next generation airborne system, known as the Hyperspectral Digital Collection Experiment (HYDICE), is under development and is being administered by the Naval Research Laboratories under the Congressional Dual Use initiative. HYDICE covers the spectral range 0.4 to 2.5 μm, with a spectral resolution of 10 μm. The design altitude of HYDICE is lower than AVIRIS (6 km vs. 20 km) but this enables a spatial resolution of 3 m over a 936 m swath width. The HYDICE uses a single 320 x 210 element indium antimonide detector array thus making possible a potentially much simpler and lower cost system than AVIRIS.

In addition to the AVIRIS and HYDICE systems, which are the product of funded government programs, there are also several mulispectral airborne imaging systems that are available for commercial rental. These systems typically provide spectral channels similar to those available in the present satellite imagers.

4.3 Aircraft Remote Sensing - Active Depth Resolved Systems

Active airborne remote sensing systems also have the potential to measure ocean parameters as a function of depth. The AOL has demonstrated this capability by the use of the on-frequency direct backscatter to measure relative sediment concentration as a function of depth.

A potential also exists for the use of active airborne lidar systems, such as the AOL, to measure additional ocean properties as a function of depth by means of short laser pulse illumination and time resolved receivers. Such systems would include fluorosensing systems to provide specie information and Raman and Brillouin systems to provide temperature, salinity, sound speed and diffuse attenuation coefficient profiles.

4.3.1 Brillouin Scattering - Diffuse Attenuation (K) and Backscatter Measurements (b_b)

The K and b_b measurement functions are accomplished in the following manner. A pulsed laser illuminates the water from above and then a receiver in the aircraft detects and analyzes the Brillouin and the on-frequency (Mie and Rayleigh) backscatter produced by the beam as a function of depth. The signal processor derives the diffuse attenuation coefficient (K) from the Brillouin signals at successive depths. The backscatter coefficient b_b is derived by normalizing the Mie signal to the Brillouin signal at each depth.

Using the definition of K as the slope of the vertical profile of the logarithm of downwelling irradiance, the value of K can be derived from the Brillouin backscatter measurements in the following way.

$$E_R(D_1) = F(H + D_1)^{-2} \exp[-2\underline{K}D_1]$$

$$E_R(D_2) = F(H + D_2)^{-2} \exp[-2\underline{K}D_1 - K\Delta D]$$

where

$E_R(D_1)$ = Brillouin signal received from scattering at depth D_1
$E_R(D_2)$ = Brillouin signal received from scattering at depth D_2
H = height of transmitter/receiver above the ocean surface
D_1, D_2 = two different depths
ΔD = $D_2 - D_1$
$\underline{K}$ = average diffuse attenuation coefficient from surface to D_1
K = diffuse attenuation coefficient in the depth interval ΔD
F = a constant which includes laser power, the Brillouin scattering cross section, system parameters and efficiency factors

Solving for K, the following expression is obtained.

$$K = \left\{ \ln\left[E_R D_1 / E_R D_2 \right] - \ln\left[\frac{H + D_1}{H + D_2} \right]^2 \right\} \left(\frac{1}{2\Delta D} \right)$$

The following Table 4-4 summarizes the results of calculations that show the depth that can be achieved with 20% or better accuracy in K as a function of KD, K and $\Delta K/K$ under both moonlight and sunlight conditions.

Table 4-4 Brillouin Diffuse Attenuation Measurement Performance

	Moonlight	Moonlight	Moonlight	Sunlight	Sunlight	Sunlight
K (m^{-1})	$\Delta k/D$ (%)	D (m)	KD	$\Delta K/K$	D (m)	KD
0.03	20.3	160	4.8	20.3	95	2.85
0.05	20.3	100	5	24.4	60	3
.1	18.7	50	5	20.3	30	3

These calculations have assumed the following systems parameters:

Laser energy per pulse = 0.1 J
Receiver Area = 0.07 m^2 (12-inch diam.)
Receiver efficiency = 0.7
Aircraft Altitude = 300 m
Depth Resolution = 5 m

Brillouin scattering is used because it is an intrinsic property of the water itself. The scattering coefficient for the Brillouin process is known and is essentially independent of both the temperature (although the frequency of the scattered light is temperature dependent - see below) and the particulate loading of the water. The technique of using Brillouin backscatter to obtain K profiles is disclosed in U. S. Patents 4,986,655 and 4,986,656 by Sweeney, Leonard and Titterton [Sweeney, 1991]. The rights to these Patents, which are reproduced in Appendix B, are held by EOO, Inc.

A necessary component of a Brillouin scatter ocean water lidar is a narrow band receiver that enables a wide field of view. Such a receiver is the integrating sphere Fabry-Perot that is disclosed in U. S. Patent 4,907,887 by Leonard and Sweeney. The rights to this Patent, which is also reproduced in Appendix B, are also held by EOO, Inc.

4.3.2 Brillouin Scattering - Temperature (Sound Speed) Measurements

The frequency shift of the Brillouin scattered light is an essentially linear function of the velocity of sound in the water. The same receiver that is described above for diffuse attenuation measurements can be adapted for frequency shift measurements. The sensitivity is such that measurements of ±1 °C are readily made to depths of 3 to 5 diffuse attenuation lengths. Laboratory measurements have shown that the use of stimulated Brillouin scattering (SBS) can achieve temperature accuracy at the ten millidegree (0.01 °C) level [Leonard and Sweeney, 1988].

4.3.3 Fluorescence Measurements

The Raman and Brillouin scattering processes are essentially instantaneous. Fluorosensing systems, however, would be limited by the fluorescence decay time of the species being sensed. For Raman and Brillouin systems the backscatter is instantaneous and the depth resolution is then only a function of the laser pulse duration. After a few attenuation lengths multiple scattering causes path ambiguity which ultimately limits the depth resolution at deeper depths.

4.4 Aircraft Remote Sensing - Combined Passive and Active Systems

The NASA Oceanographic Airborne Lidar (AOL) is a multichannel lidar fluorosensor that has been configured [Hoge, 1986] to function simultaneously as a passive spectroradiometer for measuring upwelling ocean color radiance. The resulting spectroradiometer has both active and passive ocean color measurement capabilities. The sensor has 32 contiguous but separate spectral bands which cover the spectral region from 350 to 800 nm. When operating in active lidar mode the AOL typically uses

a 532 nm laser source producing a 15 ns pulse at peak power of 3 MW and a pulse repetition rate of 6.25 pps.

Active-passive ocean color sensing is defined as the combination of both passive and active detection and quantification capabilities within a single sensor. Such an instrument retains all the important characteristics of each separate detection scheme while simultaneously functioning without detectable interaction between each mode. The application of the AOL in active-passive mode was first applied to chlorophyll measurements [Hoge, 1986]. The chief benefit was found to be the data fusion and resulting benefit which was not achievable by the separate passive or active sensor individually.

The distinct and important characteristic of the active or laser--induced spectra is its specificity. The laser's spectral bandwidth (typically subnanometer) allows excitation of spectral lines which are easily resolved and unambiguously assigned to chlorophyll and phycoerythrin pigments in the phytoplankton and Raman scatter from the surrounding water molecules. The importance of the laser induced scattering from the Stokes, 3300 cm^{-1} OH stretch water Raman line should be emphasized. Rather large variations in the penetration depth of the laser illumination can exist, especially in the coastal waters of interest. If left uncorrected this spatial variability in water column optical attenuation would manifest itself as variability in the pigment fluorescence signal observed. Since the Raman scatter is due only to liquid water molecules the relative penetration depth may be defined by the strength of this spectral line. Thus the apparent variation of pigment fluorescence caused by water column optical attenuation can be corrected by normalization using the water Raman backscatter signal. [Bristow, 1981]. The quantitative measurement of chlorophyll by laser fluorosensing is discussed in detail in Section 5.2.1.

4.5 In situ Measurements

Modern technological advances in optics and electronics have revolutionized the design and utility of many classical analytical techniques, such as spectrometry, chromatography, etc. Therefore it is important to consider whether these improvements might provide the necessary capabilities for in situ measurements as part of a coastal water properties reconnaissance system. Because of the limited resources of this program, evaluation has been restricted to several specific techniques which are either being developed or are well established tools. In general, in situ optical techniques are

favored since they are easily adapted to automated field use and the critical optical properties can sometimes be derived directly from the optical measurement itself.

4.5.1 In situ Measurement of Sediment

Both the suspended sediment concentration and the sediment particle size distribution are important determinants of the optical properties of water. Various sampling and subsequent analysis methods have been developed for particle sizing in general, including sieving, microscopy, gravity and centrifugal separation, etc. A convenient summary of particle size analysis techniques is given in the Particle Sizing Seminar, Notes and Workbook by Horiba Instruments, Inc. [Horiba, 1992].

The origins of modern optical in-situ instrumentation can be traced to Austin and Petzold's [Austin, 1975] measurement of the volume scattering function. Optical methods for particle concentration and size measurement have now been developed into practical tools for analysis of water samples. The principle of operation is the following. Light irradiating a suspension of particles in water is scattered at various angles. If the particles are comparatively large, the scattering tends to be concentrated in a forward direction. As the size of the particle decreases more light is scattered away from the forward direction. Scattering out of a beam (assuming the scattering is axi-symmetric) is given by

$$b = \iint \beta(\theta) d\Omega = 2\pi \int_0^{\pi} \beta(\theta) \sin\theta d\theta$$

where

$\beta(\theta)$ = volume scattering function (VSF), $m^{-1}sr^{-1}$
b = volume scattering coefficient, m^{-1}
b_b = backscatter coefficient, obtained by evaluating $\beta(\theta)$ at $\theta = \pi$, $m^{-1}sr^{-1}$

Typical commercially available instruments that make VSF measurements are listed in Table 4-5. Special purpose devices developed as one-of-a-kind instruments may also be considered and are described in the literature [refs.].

Table 4-5 Commercially Available Optical VSF Instruments

Manufacturer	Northwest Research Associates, Inc. Bellevue, WA	Horiba Kyoto, Japan
Model Number	LISST-1000	LA-900
VSF Angle Range	0.85 mr to 85 mr	not available
Source Wavelength	"red"	623.8 nm and "white"
Utilization	Laboratory	Immersible in-situ
Particle Size Range	5 - 500 micron diam.	0.04 - 1000 micron diam.

The principal limitation of the above instruments is the lack of VSF measurement in the angle range near backscatter. In contrast limited situations, the backscatter coefficient, b_b, is the controlling optical property for operational systems. For deep penetrating imaging systems (which are usually range gated), the total extinction and the point spread function (derivable from the forward portion of the VSF) are the controlling optical properties. An in situ instrument that simultaneously measures the total extinction and the complete VSF, including both narrow angle forward scatter and backscatter, is currently under development by EOO, Inc. and Global Associates under Navy Phase II SBIR funding. The parameters of this instrument are listed in Table 4-6.

Table 4-6 Extinction/VSF Instrument Currently Under Development

Function	measurement of beam attenuation coefficient (c) and volume scattering function (VSF)
Dynamic Range	VSF: 0.0001 to 10,000 $m^{-1}sr^{-1}$ c: 0.05 to 2 m^{-1}
VSF angular measurements	0.1° to 5° : 0.1° increments 175° to 180° : 0.1° increments 45°, 90° and 135° : each over ≠ 5° range
Wavelength	532 nm
Integration Time	≈ 1 sec
Depth	Surface to 200 m

4.5.2 In situ measurement of Chlorophyll and Dissolved Organics

Modern analytical methods for determining chlorophyll and dissolved organics typically use optical absorption and/or fluorimetry. In the absorption method the sample

is irradiated at several wavelengths and the absorption spectrum is determined. With fluorimetry the water sample is excited at one wavelength and the resulting fluorescence emission spectrum is observed at other wavelengths.

A commercially available absorption instrument for in situ direct immersion measurements is described in Table 4-7.

Table 4-7 Commercially Available Chlorophyll Absorption Meter

Manufacturer	Western Environmental Technology Laboratories, Inc.
Model Number	AC-10
Chlorophyll Dynamic Range	0-1000 µg/l
Precision	0.05 µg/l @ 12 Hz 0.015 µg/l @ 1 Hz
Spectral Range	410 - 850 nm
Number of Wavelengths	10
Utilization	In Situ Immersion

5.0 Quantitative Optical Remote Sensing

In this section we attempt to match the requirements for the coastal water properties with the capabilities of the available and potential optical remote sensing measurement techniques to provide the required information.

5.1 Satellite Optical Sensors

We have evaluated the suitability of satellite passive optical sensors for coastal water quality predictive model initialization and update. The "suitability" is comprised of:

- resolution (pixel size)
- sensitivity including SNR, and noise equivalent radiance
- spectral bands including placement, width, and number
- swath width and placement
- orbit parameters such as revisit time
- data availability

In general remote sensing in the coastal zone requires higher spatial and temporal resolution than has been developed for open ocean sensors. The sensitivity and placement of bands can be inferred from the previous work with the existing satellite and airborne sensors.

5.1.1 Sea Viewing Wide Field-of-view Sensor (SeaWiFS)

The Nimbus-7 Coastal Zone Color Scanner (CZCS) was the first instrument to acquire ocean color data from space [Hovis, 1980]. Although envisioned as a proof-of-concept sensor with only four visible spectral bands and a limited recording capability, the CZCS provided high quality imagery from the autumn of 1978 until the summer of 1986. The use of CZCS data has largely focused on the spatial and temporal distribution of pigments, with the length scales being mesoscale, basin and global. In addition there have been relatively limited attempts at quantitative algorithm development to relate the water-leaving spectral radiance to biological or optical parameters such as pigment concentration and diffuse attenuation. Examples of such work are that of Gordon and co-workers [Gordon, 1980] and Austin and Petzold [Austin 1981; Austin 1986].

Following the success of CZCS, a follow-on ocean color space sensor, the SeaWiFS, was designed by NASA. The specifications for the spectral bands of the SeaWiFS sensor [Hooker, 1992] are listed in Table 5-1. The signal-to-noise ratio (SNR)

listed for each band of the SeaWiFS in Table 5-1 will be used as the baseline required SNR value for a satellite sensor.

Table 5-1 Instrument Parameters of the SeaWiFS Sensor

Band	Wavelength FWHM (nm)	Saturation Radiance[1]	Input Radiance[1]	SNR
1	402-422	13.63	9.10	499
2	433-453	13.25	8.41	674
2	480-500	10.50	6.56	667
4	500-520	9.08	5.64	640
5	545-565	7.44	4.57	596
6	660-680	4.20	2.46	442
7	745-785	3.00	1.61	455
8	845-885	2.13	1.09	467

Note 1. Units of mW cm^{-2} μm^{-1} sr^{-1}

Although the pixel size of the SeaWiFS at 1.1 km is much greater than the 10 to 30 m spatial resolution that is required for coastal water remote sensing, both the photometric sensitivity and the spectral band placement of the SeaWiFS can be taken as guidelines for the required SNR and the minimum wavelength set that is needed for a sensor with higher spatial resolution. In addition, even though the SeaWiFS is not capable of sensing the coastal zone itself, with adequate spatial resolution, the information obtained from SeaWiFS may be useful to a predictive model by measuring the open ocean physical parameter boundary values that help to define the ocean physical properties in the coastal zone. For example, if the coastal zone is taken to be 50 km in extent, a spatial resolution of $\approx$ 1 km at the outer boundary would be reasonable.

Selection of the SeaWiFS bands by the NASA design team was based on the spectral absorption characteristics of some common in-water optical constituents, mean extraterrestrial irradiances, and spectral transmittance of the atmospheric constituents.

The difficulty associated with satellite measurement of water-leaving radiance is illustrated in Figure 5-1, which is a plot of water-leaving and satellite observed radiances as a function of wavelength with chlorophyll concentration as a parameter [Hooker, 1992]. The radiance data shown is for a cloud free atmosphere modeled by Gordon. Figure 5-1 also shows the sensitivities for the sensors on CZCS, SeaWiFS, and MODIS.

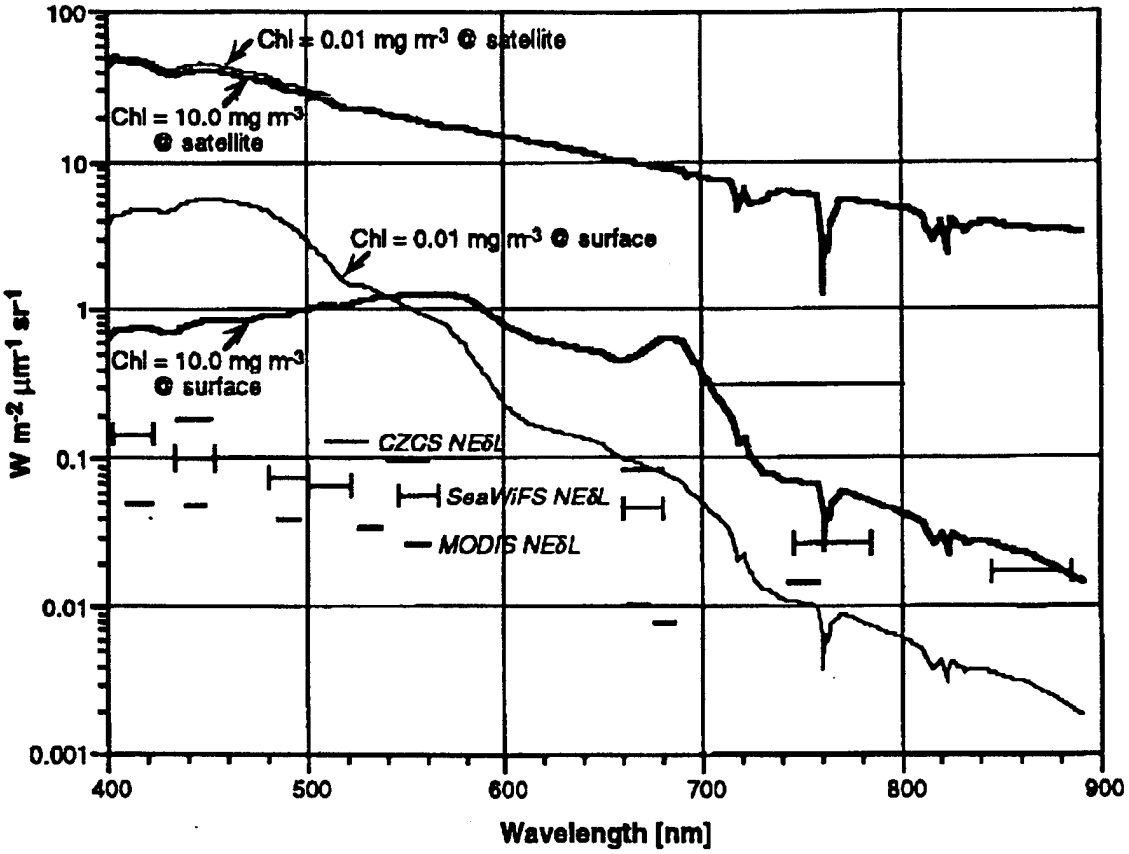

Figure 5-1 Spaceborne Sensor Sensitivity vs. Water-Leaving Radiance
(Appears as Figure 3 in Vol. 1 of NASA SeaWiFS Technical Report Series, July 1992.)

Figure 5-1 shows the expected water-leaving radiance for chlorophyll at concentration levels of 0.01 mg/m^3 and 10.0 mg/m^3. The top set of curves on Figure 5-1, which are above a value of 10 W m^{-2} µm^{-1} sr^{-1} on the sensitivity scale, show the radiance received at the satellite. Since the atmospheric path radiance is ≈ 90% of the radiance received at the satellite the curves appear on the log scale to be nearly independent of the water-leaving radiance. However, the retrieval of water properties, from the spectral characteristics of water-leaving radiance, requires that the small water-leaving radiance signals be correctly determined.

The placement of the SeaWiFS bands and the radiometric sensitivity of its sensors were selected by the NASA design team so that chlorophyll could be measured with adequate precision. This of course assumes that chlorophyll is the dominant source of

ocean color, i.e., water that in general is not coastal and therefore is unlikely to contain significant amounts of either sediment or dissolved organic matter. It should be noted that on Figure 5-1 the sensitivity of the SeaWiFS is at least a factor of 10 more sensitive than the chlorophyll water-leaving radiance level.

A requirement for successful utilization of the SeaWiFS data (or any satellite or high altitude aircraft remote sensing data) is that the atmospheric path radiance correction be properly accomplished. Methods have been developed to characterize atmospheric scattering for various degrees of atmospheric turbidity relative to a clear, Rayleigh atmosphere. [Gordon, 1978] The path radiance can be taken into account by noting that there is a relationship between the radiance at various wavelengths for a given degree of turbidity. Since water is highly absorbing in the red to near infra red, most of the signal received at the satellite sensor at these wavelengths is due to sky radiance and not water-leaving radiance. Establishing the radiance ratio between these bands then permits the appropriate correction to be made to the received signals in the blue and green bands.

A very serious problem with SeaWiFS is the light collection and focal plane design which permits light scattering internal to the instrument at very high levels due to out of field radiation . For example, when the sensor is looking within 10 pixels (11 km) of a bright coast the scattering, internal to the SeaWiFS instrument, from the bright coast will invalidate the spectral radiance data being collected from the imaged water pixel. This effect was not discovered until calibration of the device [Mueller 1995] The defect has now been mitigated to some extent but quantitative documentation as to the remaining out of field scattering was not available when this report was written.

5.1.2 Satellite Sensitivity and Pixel Size

The sensitivity of various satellites as a function of spatial resolution is shown in Figure 5-2. The two points in the upper left hand corner of Figure 5-2 indicate the performance of the SPOT and LANDSAT sensors. The solid and dashed slanted lines show the scaling of the noise equivalent radiance as the square root of the number of pixels averaged for these satellite sensors. It is thus possible by averaging over some number of pixels to improve the radiance sensitivity of the measurement at the expense of spatial resolution. The performance of the CZCS, the SeaWiFS and the MODIS satellite sensors is also shown on Figure 5-2 as generally clustering in a region which has an order of magnitude better radiance sensitivity and two orders of magnitude worse spatial resolution than SPOT or LANDSAT.

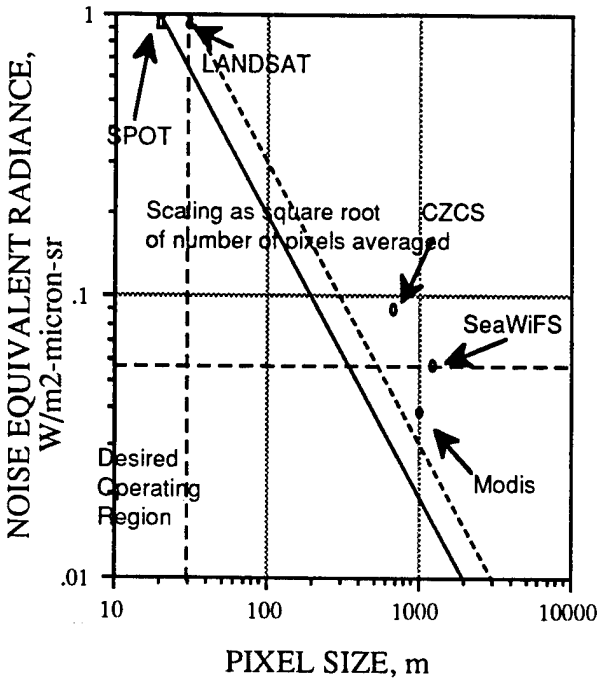

Figure 5-2 Satellite Sensitivity vs. Pixel Size

The ideal candidate for coastal water reconnaissance would have the spatial resolution of a SPOT or LANDSAT with the sensitivity of a SeaWiFS. This desired operation region is indicated in the lower left hand corner of Figure 5-2. The question can be asked: Why is the sensitivity of LandSat limited to 1 W/m^2-µm-sr? The answer is twofold: (1) the LANDSAT sensor operates with instrument limited (rather than shot noise limited) detectors; and (2) LANDSAT has a wide swath scan resulting in a low dwell time per pixel. The problem can be solved, and a satellite capable of coastal operation can be configured by (1) using a shot noise limited detector and/or (2) operating with a narrow, directable swath, with longer effective dwell time per pixel. Conceptual designs of both types of coastal water satellite sensing systems have been developed and are described in Appendices C and D of this report.

5.1.3 LANDSAT Image Processing

A LANDSAT image was analyzed to test published water physical properties retrieval algorithms on actual data, generate maps for initialization of the predictive model, and establish the processing procedures to be used on future studies. The validity of the procedure was not tested with ground truth. Because of the low intrinsic

sensitivity of LANDSAT 5 x 5 and 11 x 11 pixel averaging was used to increase the signal-to-noise ratio.

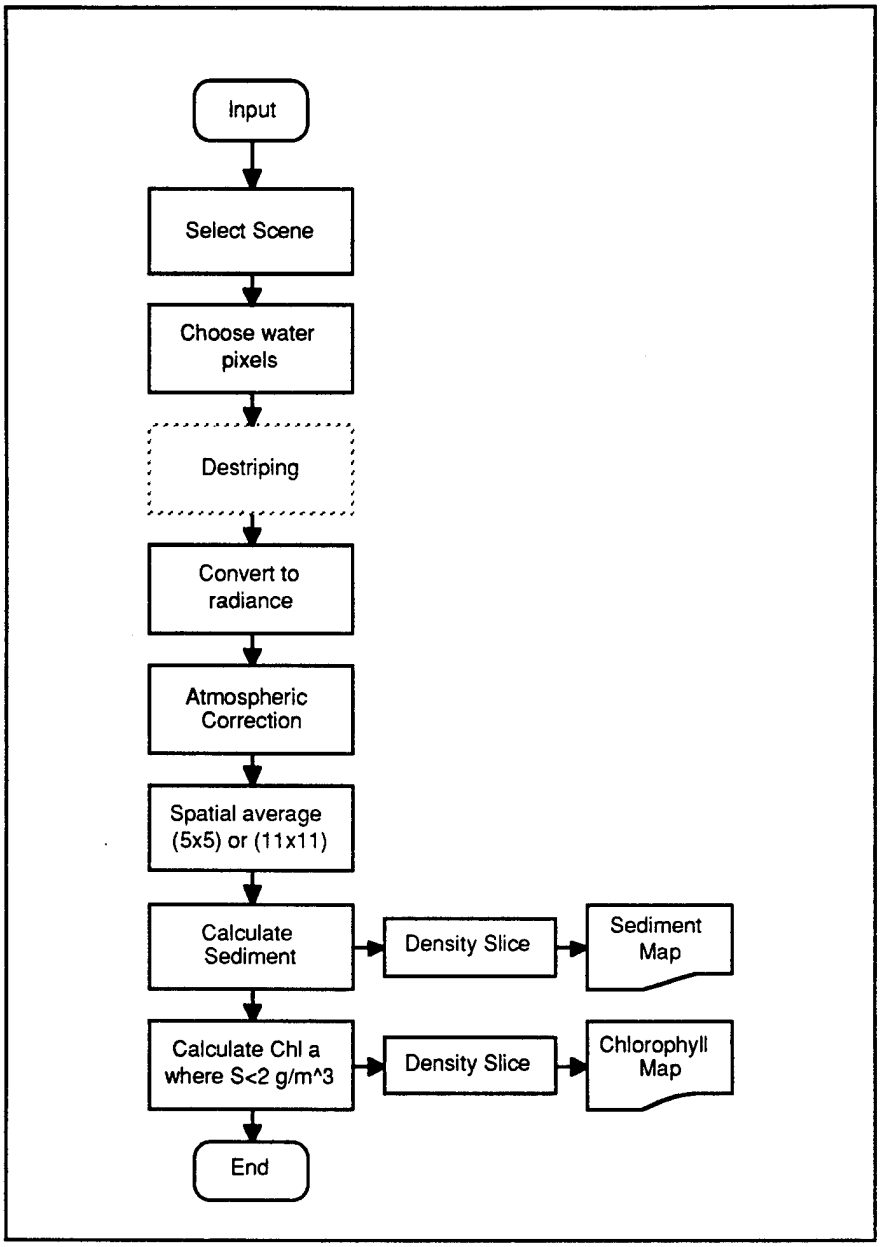

Figure 5-3 LANDSAT Image Analysis Flowchart

The image selected was coordinated with SAIC and represented a portion of the California coast which had been modeled by SAIC for prediction of water optical properties. The retrieval algorithms were programmed into a commercial image analysis package [ER Mapper, 1992]. The physical properties, chlorophyll and sediment, were displayed on a contour map in broad increments using the built-in features of the image analysis software. The procedure used in the image processing is shown in Figure 5-3.

The processing steps are discussed in more detail below.

Step 1: Input data tape into image processing application

Data from the TM10 sensor on the LANDSAT 5 satellite was acquired from Eosat [Earth Observation Satellite Company, 4300 Forbes Blvd., Lanham, MD.] in a 7–band, map-oriented format. In this format the raw, path-oriented LANDSAT data is geometrically altered to correspond to latitude-longitude coordinates. The image shows sediment outflow from the Santa Margarita river along the coast of southern California on January 23, 1993.

Step 2: Select a sub-scene of test area

The sub-scene, consisting of 737 x 668 pixels, covers the Santa Margarita river, which is the test area considered in the predictive model. The sub-scene includes on-shore landmarks for rectifying the image for GIS purposes, the river mouth features, and the straight coast-line showing the surf zone. The region of analysis could be expanded, but this minimum size sub–scene was chosen to reduce the processing time.

Step 3: Choose water pixels

The water pixels were selected to allow the software to build contour maps only in the regions valid for the algorithms. Boundaries were drawn by hand along the coast using a visual delineation in the three visible bands. Likewise, harbors, piers and spits of land were distinguished from the water pixels. An automated procedure to select the desired water pixels could be implemented using TM band 7 since water is dim in the infrared bands. The atmospheric correction must be done first to eliminate the aerosol scattering contribution and high sediment loading in the water may confuse this advanced procedure.

Step 4: De-striping and de-blooming

The Thematic Mapper sensor consists of a number of detectors per band and the calibration of these individual detectors can drift over time. A de-striping procedure can be used to correct the gain and offset of the detectors [Jensen, 1986, Richards, 1986]. This fine structure was not apparent in the data in our scene so this procedure was not implemented.

Another artifact in the data is an apparent blooming of the detectors after passing from a bright object (land) to a dim object (water). The physics of the effect is that when the scanner sweeps across a bright edge (i.e. goes from over land out to over the ocean) there is a saturation effect that persists and causes the sensor to be less

sensitive over the water than when the scanner is scanning from the ocean to the land. This will cause a striping or banding effect perpendicular to the shoreline with the bright stripes being the scans toward the shore and the dark stripes being the scans away from the shore. The effect has a exp[-at] time constant with a 1/e distance of about 1000 pixels, which obviously presents a problem as we have observed. Dennis Helder of South Dakota State University has developed [Helder, 1992] in collaboration with NASA a correction algorithm for LANDSAT which may extend the utility of LANDSAT data for coastal water clarity measurements.

A further modulation along the stripes was also noted in the LANDSAT data. In a private communication Helder said it was an electrical engineering artifact in the sensor electronics. If "Level A data" from LANDSAT with the original 16 pixels was used (rather than the geo-corrected data which is transformed into 17 pixels) Helder thought it would be possible in principle to reduce the effect of this artifact.

Step 5: Convert digital number to radiance

The LANDSAT pixel data for each wavelength band is expressed in digital numbers, or counts. The water physical property retrieval algorithms require data at each pixel, in each wavelength band, expressed in radiance units. The calibration information to convert digital number to radiance is included in the header file information of each LANDSAT image. The minimum and maximum radiance is listed for each wavelength band. The pixel radiance is calculated as:

$$\text{pixel radiance} = [\text{bias} + (\text{gain} \times \text{DN})] / \text{BW}$$

where

pixel radiance is in units of (mW/cm^2 sr μm)
bias is the minimum radiance
gain = (maximum radiance) / 254 - (minimum radiance) / 255
BW is the wavelength bandwidth of each LANDSAT band
DN is the digital number recorded for each band at each pixel.

These calibration values are shown in Table 5-2 for the 23 Jan. 1993 scene. The digital numbers in the LANDSAT scene were converted into radiance units in the image processing application using these values.

Table 5-2 LANDSAT calibration parameters for 23 Jan. 1993 scene

TM band	BW	min. radiance	max. radiance	bias	gain
TM1	.066	-0.00761	1.05541	-0.00761	0.00419
TM2	.082	-0.01722	2.60578	-0.01722	0.01033
TM3	.067	-0.01228	1.63452	-0.01228	0.00639
TM4	.128	-0.02341	2.94435	-0.02341	0.01150
TM5	.217	-0.00493	0.68522	-0.00493	0.00272
TM7	.252	-0.00310	0.42549	-0.00310	0.00169

Step 6: Atmospheric correction

The standard method of correcting the satellite received signals for atmospheric scattering, using near infra red bands that are highly absorbed in water, was discussed previously. This method uses TM5 and TM7 bands to evaluate the wavelength scaling of aerosol scattering. Since the LANDSAT sensor has limited SNR, a 25 x 25 grid of pixels is averaged to calculate the correction factor.

A simpler method of atmospheric correction assumes that the minimum radiance is due to atmospheric scattering; and the value of R_{min} is subtracted from the radiance value at each pixel. A histogram can be constructed of the number of pixels versus pixel radiance for each wavelength band of the water portion of the LANDSAT scene to find the value of R_{min}. A typical result is shown in Figure 5-4.

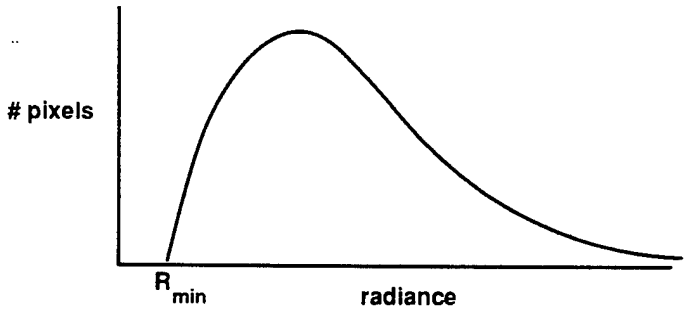

Figure 5-4 Typical radiance histogram

Errors in this procedure may be due to variation of aerosol density across the scene and from non-zero minimum radiance in the scene. A higher aerosol concentration will lead to greater radiance from the atmospheric path, which is not corrected by subtracting R_{min}. A non-zero scene radiance implies that the R_{min} value is due to atmospheric radiance plus real information from the scene. Small errors in the atmospheric correction can be tolerated since we are looking for only broad classification of the water physical properties. The reduced SNR of the sensor and applicability of the locally-derived algorithm also limit the accuracy of the measurement.

Step 7: Spatial averaging to improve SNR

As discussed in Section 5.1, the noise-equivalent radiance of the Thematic Mapper sensor is 0.1 mW/cm^2 sr μm. If we apply the sediment formula to this minimum detectable radiance, we find the minimum detectable sediment concentration is 2.2 g/m^3. A spatial averaging procedure is available in the image analysis software to generate a running average of the pixel values over a specified grid. The central pixel in a 5 x 5 or 11 x 11 grid is assigned the average of the 25 or 121 surrounding pixels. This procedure should increase the SNR by a factor of 5 or 11 so the minimum detectable sediment concentration is 0.44 or 0.2 g/m^3, respectively.

Step 8: Calculate sediment concentration

The sediment concentration is calculated according to the algorithm as described in references [Tassan, 1987, Ekstrand, 1992]. The formula is applied to the data after all the preceding steps of de-striping, radiance calibration, atmospheric correction, and spatial averaging.

$$\log(S) = 2.7 + 1.06 \log(k(TM3) * L_{TM3}),$$

where

S = sediment concentration in g/m^3

$k(TM) = \frac{\pi n^2}{(1-\rho)F_0(TM)\cos\theta}$ converts the LANDSAT radiance to reflectivity

n = index of refraction of water

ρ = reflectivity of water

F_0 (TM)= TM solar constant; [Gordon, 1983]

θ = solar zenith angle (62° for 1/23/93 scene)

L_{TM} = Thematic Mapper pixel radiance in mW/cm^2 sr μm

Using the appropriate parameters, including the solar zenith angle tabulated in the LANDSAT image header, we can evaluate the reflectivity expression for the LANDSAT bands: k(TM1) = .062; k(TM2) = .062; k(TM3) = .062; k(TM4) = .054

The formula was applied to the 5 x 5 spatially averaged data and contour maps generated in steps of 0 - 2, 2 - 5, 5 - 8, 8 - 11 and > 11 g/m^3. The result is shown in Figure 5-5. The same formula was also applied to the 11 x 11 averaged data with the product shown in Figure 5-6. Some loss of detail is apparent in the 11 x 11 image (notice the broadening of the surf zone), but the general contours are similar. This result gives some confidence that the calculation is not adversely affected by sensor noise.

Step 9: Calculate chlorophyll concentration

The chlorophyll concentration is calculated according to the algorithm that is also described in the work by Tassan and Ekstrand [Tassan, 1987, Ekstrand, 1992]. The formula is applied to the data where the sediment concentration is < 2 g/m^3 after all the preceding steps of de-striping, radiance calibration, atmospheric correction, and spatial averaging. The radiance-ratio algorithms for chlorophyll a have a high correlation to the actual chlorophyll a concentration in Case I water. If the application of the algorithm is restricted to pixels having low sediment concentration this condition may be met. Certainly the concentration of dissolved organic matter may interfere with detection of chlorophyll a and reduce the validity of the calculations. If DOM co-varies with sediment (due to run-off), the restriction of the radiance-ratio algorithm to low sediment pixels might also reduce interference of DOM.

The formula for calculating chlorophyll concentration is:

$$\log(C) = -0.057 - 2.73 \log[(L_{TM1} * k(TM1)) / (L_{TM2} * k(TM2))],$$

where

C = chlorophyll concentration in mg/m^3

$k(TM) = \frac{\pi n^2}{(1-\rho)F_0(TM)\cos\theta}$ converts the LANDSAT radiance to reflectivity

n = index of refraction of water

ρ = reflectivity of water

F_0 (TM)= TM solar constant; see reference [Gordon, 1983]

θ = solar zenith angle (62° for 1/23/93 scene)

L_{TM} = Thematic Mapper pixel radiance in mW/cm^2 sr μm

The formula was applied to the 5 x 5 spatially averaged data and contour maps generated in steps of 5 mg/m^3. The result is shown in Figure 5-7 The same formula was also applied to the 11 x 11 averaged data with the product shown in Figure 5-8. Outside of the small patches adversely affected by the sensor blooming, no area of the scene shows a chlorophyll concentration greater than 5 mg/m^3.

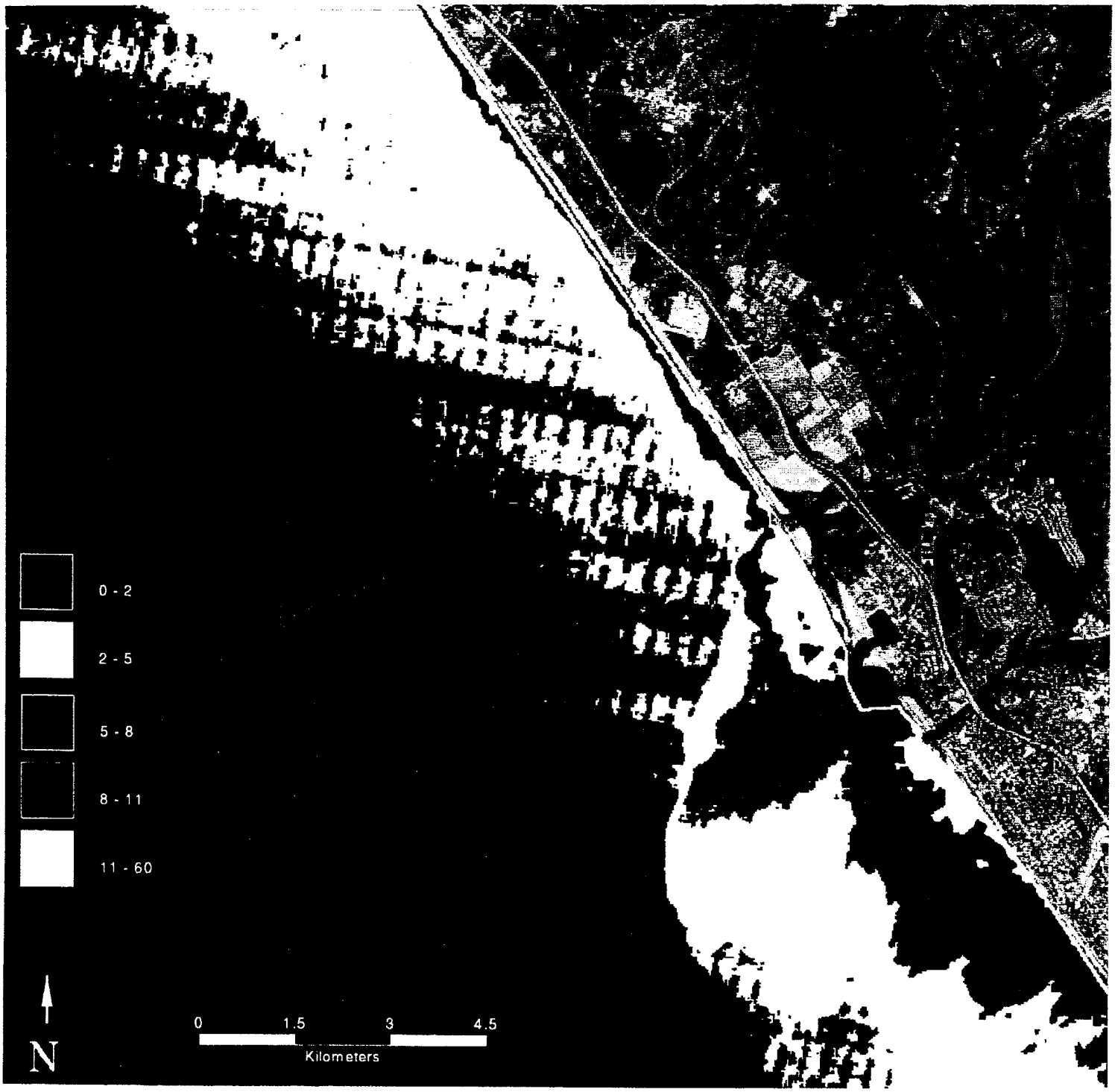

Figure 5-5 Sediment Contour Map from LANDSAT - 5 x 5 Pixel Average

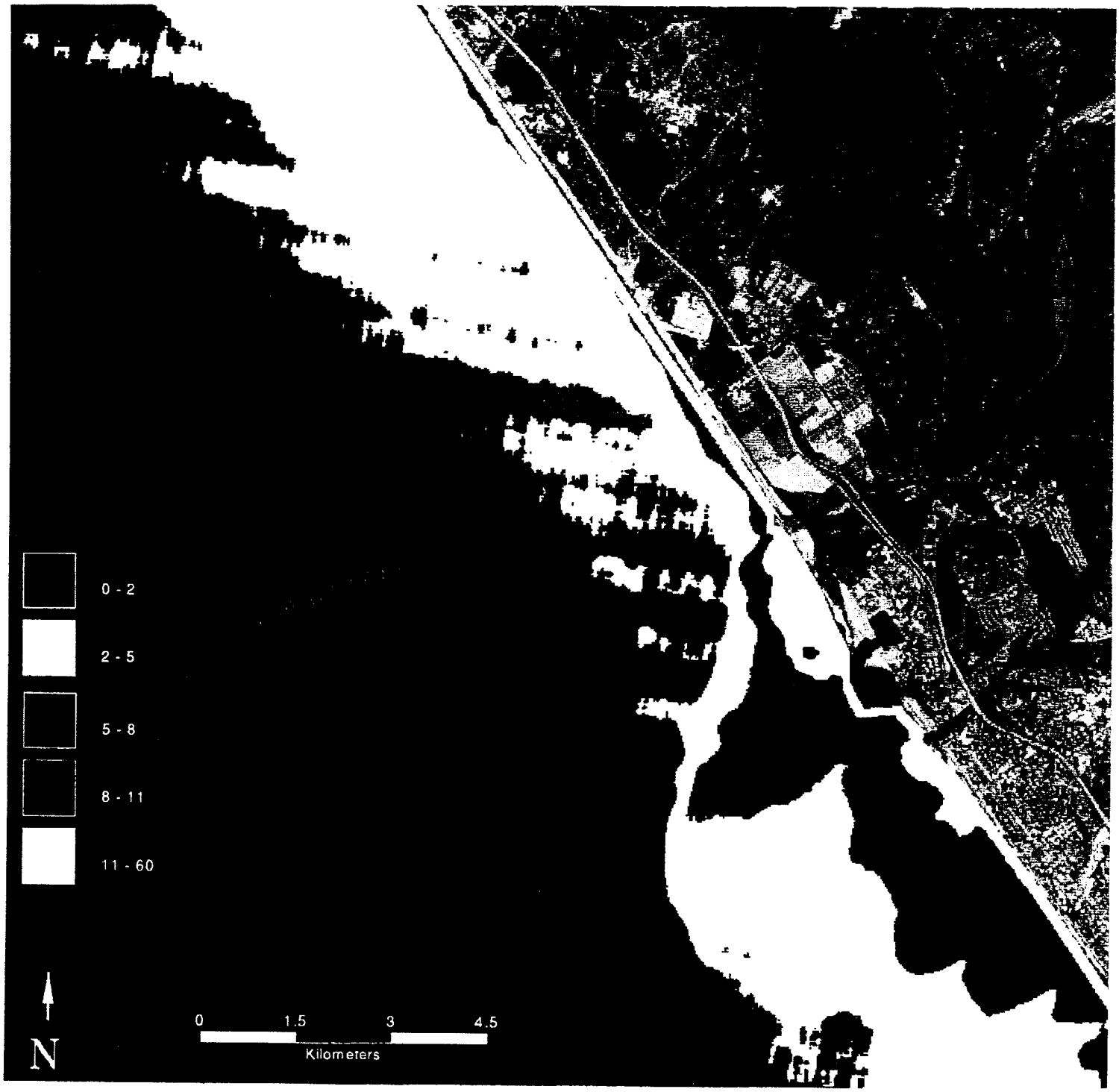

Figure 5-6 Sediment Contour Map from LANDSAT - 11 x 11 Pixel Average

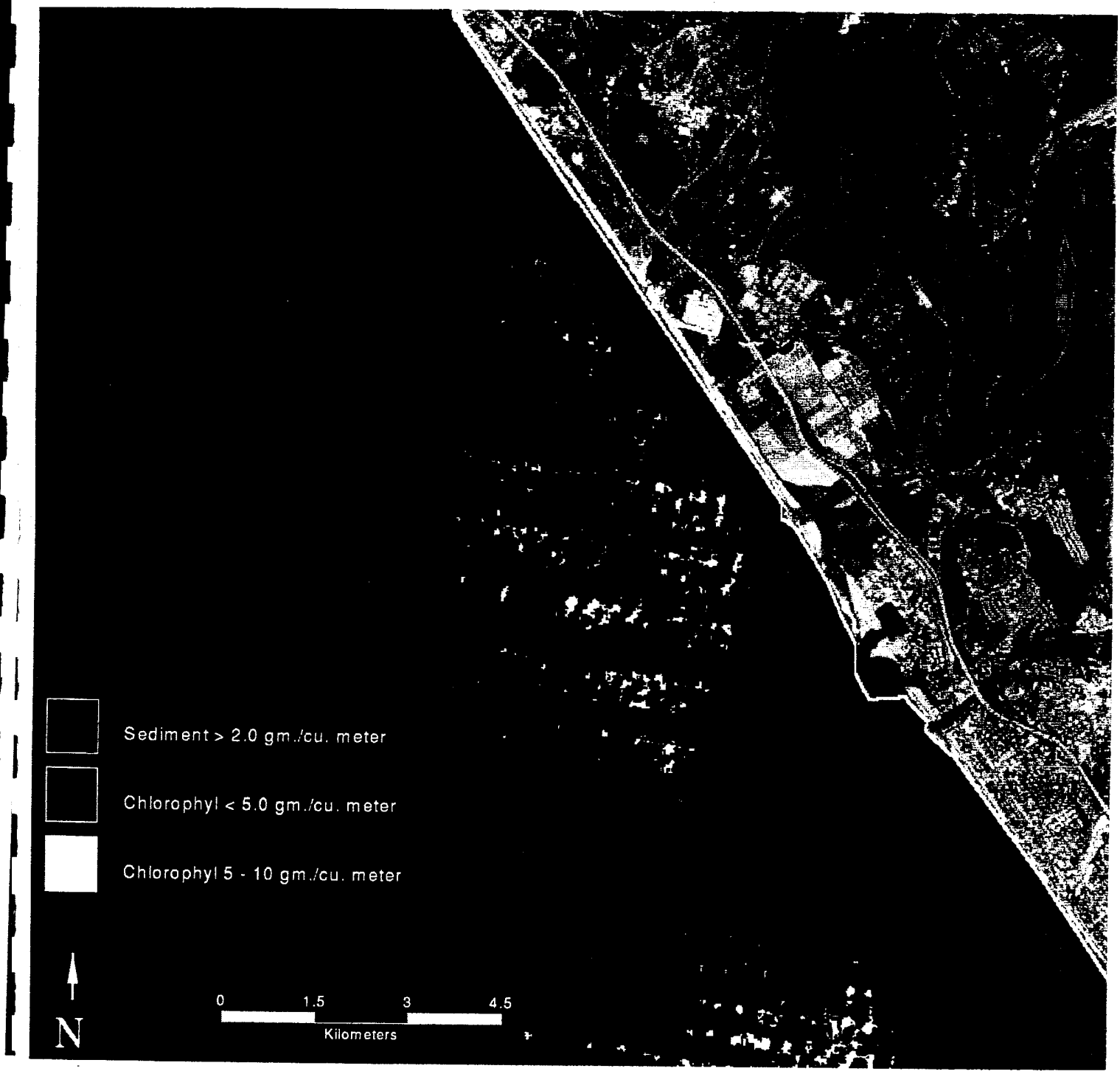

Figure 5-7 Chlorophyll Contour Map from LANDSAT - 5 x 5 Pixel Average

Conclusion:

We have used published water physical properties retrieval algorithms on actual LANDSAT data. An anomalous striping due to a sensor blooming effect was found. The structure of suspended sediment from river run-off was shown, with 5 x 5 spatial averaging needed to get $S < 2$ g/m^3. Physical sampling should be used to validate the calculation procedure at the local site.

A radiance-ratio algorithm derived for Case I water was applied to the LANDSAT data in regions where the sediment loading was small. No features in the Chlorophyll a concentration were observed on the coarse scale assumed to be valid with the low SNR achievable with the Thematic Mapper sensor. No attempt was made to simultaneously extract the sediment, DOM and chlorophyll concentrations. Again, physical sampling at the local site should be used to validate the empirical algorithm.

Advanced atmospheric correction methods using the NIR Thematic Mapper bands should be applied to check validity of the simple approach.

5.2 Aircraft Optical Remote Sensing

An aircraft platform provides a unique opportunity that is not available with satellites, i.e., the ability to use an active, laser illuminator system to achieve quantitative measurement of water properties. The following describes the use of laser fluorosensing for the quantitative determination of chlorophyll concentration. The same basic approach is currently being extended to the remote quantitative measurement of dissolved organic from aircraft.

5.2.1 Fluorosensing of Chlorophyll

Airborne laser chlorophyll fluoro-sensors typically employ downward looking pulsed lasers to excite fluorescence in the chlorophyll distributed in the water volume [Browell, 1977]. The intensity of the received fluorescence signal is used as a direct measure of the concentration of the chlorophyll. A problem with the basic technique exists because of large variations in the penetration depth due to changes in optical attenuation of the water as a function of horizontal distance. This interference can be eliminated by normalizing the fluorescence signal with the concurrent water Raman signal [Bristow, 1981].

In a series of landmark airborne field test experiments at lake Mead, Bristow showed that the laser induced fluorescence to Raman signal ratio was highly correlated (linear correlation coefficient r=0.995) with independent ground truth measurements

over a concentration range from 5 to 50 μg/l. of chlorophyll. A flashlamp pumped dye laser operating at 470 nm was used as the source. Interference filters centered at 560 nm and 685 nm were used in the receiver to isolate the water Raman and chlorophyll bands respectively.

5.2.2 Radiance Ratio Algorithms for Chlorophyll Determination

One model used to calculate chlorophyll concentration is the algorithm developed by Gordon [Gordon, 1980]. The model calculates the ratio of radiance in two bands and the result is empirically fit to ground truth measurements. The least squares fit correlation is used as a measure of the applicability of the model. In oceanic waters the chlorophyll concentration is low (< 1 μg/l) and the best bands to use are in the blue-green. The reflectivity is more sensitive in the blue because the absorption is highest. In coastal water the chlorophyll concentration is higher (> 1 μg/l) and the best bands to use are in the green and red.

A unique experimental study of the radiance ratio method for chlorophyll determination in the New York bight was made by Hoge and co-workers [Hoge, 1987] who made radiance measurements in 32 separate but contiguous 11.25 nm spectral bands using an airborne sensor. This data was used to compute 992 radiance ratios [N(N -1)] which were then correlated with independent measurements of chlorophyll concentration obtained by the method of laser fluorosensing described in Section 5.2.1. The results were displayed on a wavelength x wavelength grid (i.e. a grid of the wavelength bands used to obtain the radiance ratio) as a contour map of the value of the coefficients obtained from the linear regression of the two-band radiance ratio against the ground truth measurement of chlorophyll concentration. Regions of high correlation coefficient on the contour plot correspond to spectral band ratio regions that are suitable for measurement of chlorophyll.

Figures 5-9 through 5-12 each show the above described contour plot for a particular flight line overlayed with the band ratio position that is available from the sensors of CZCS, SeaWiFS, LANDSAT and SPOT respectively. It can be noted that the band ratios available from CZCS, SeaWiFS and LANDSAT generally fall in regions of high correlation on the contour map. It can also be noted that the band ratio available from SPOT falls in a region of lower correlation and therefore would not be considered as useful for determining chlorophyll concentrations.

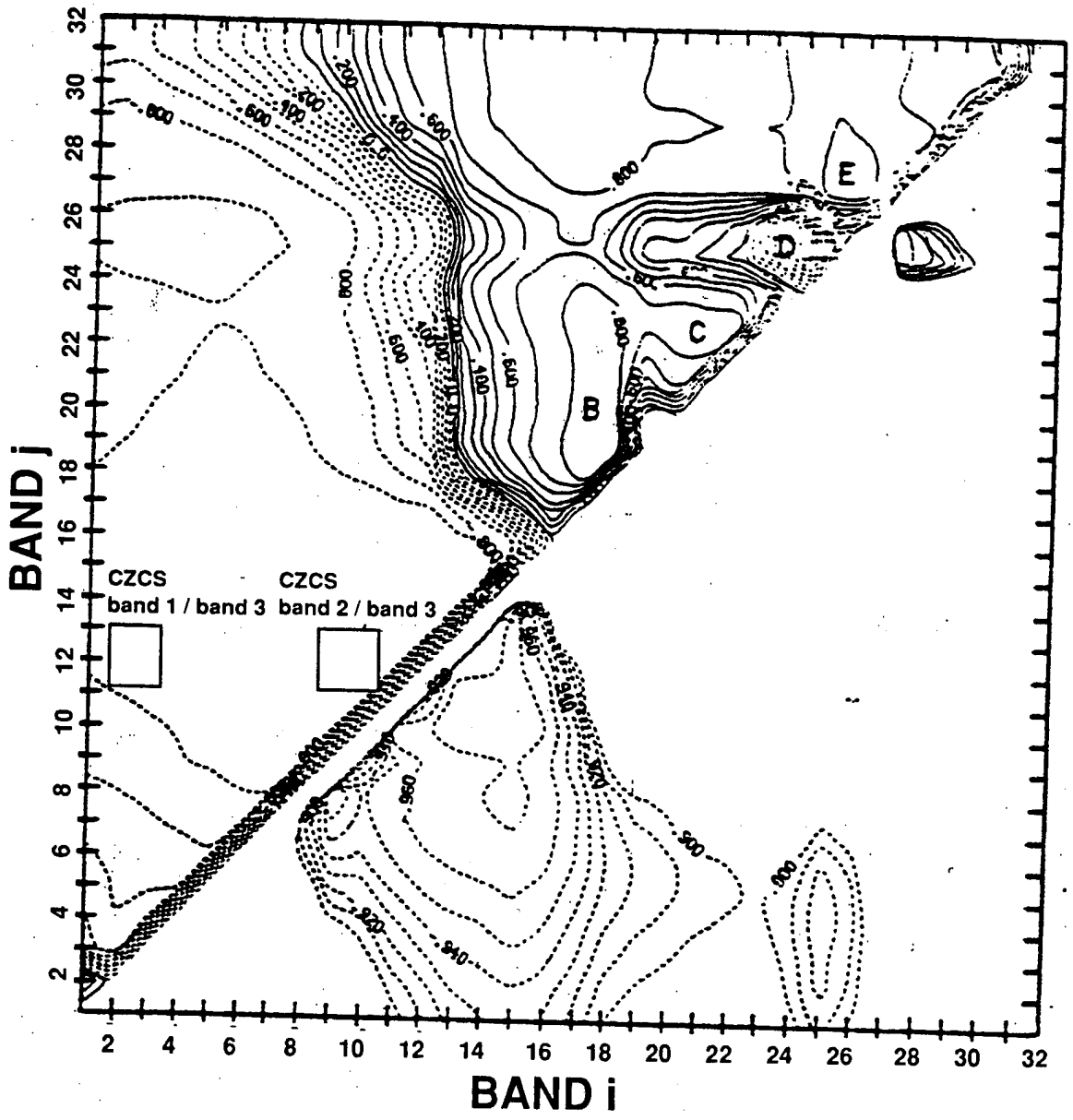

Figure 5-9 Regression Contours for Chlorophyll with Overlay of CZCS Bands

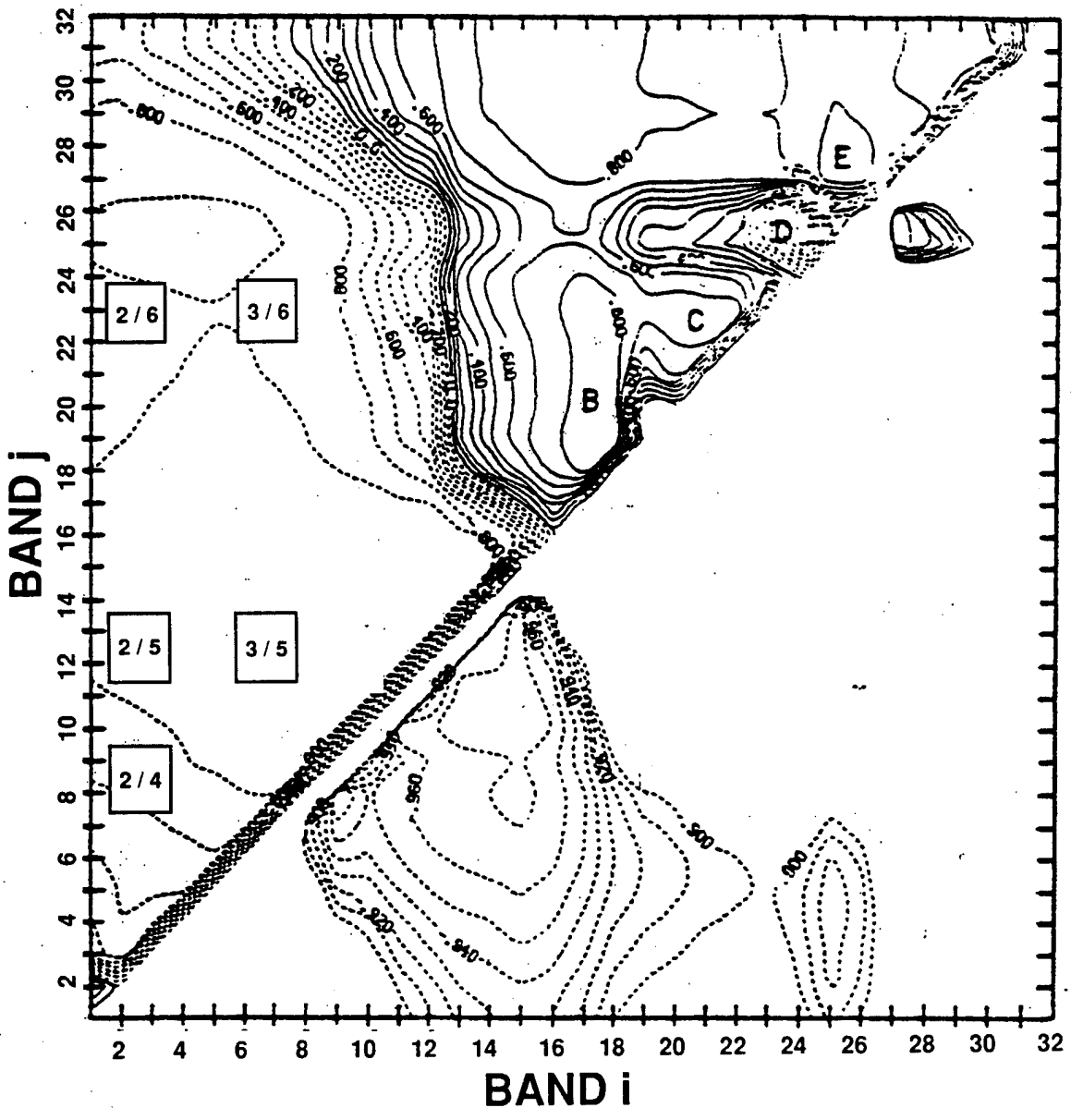

Figure 5-10 Regression Contours for Chlorophyll with Overlay of SeaWiFS Bands

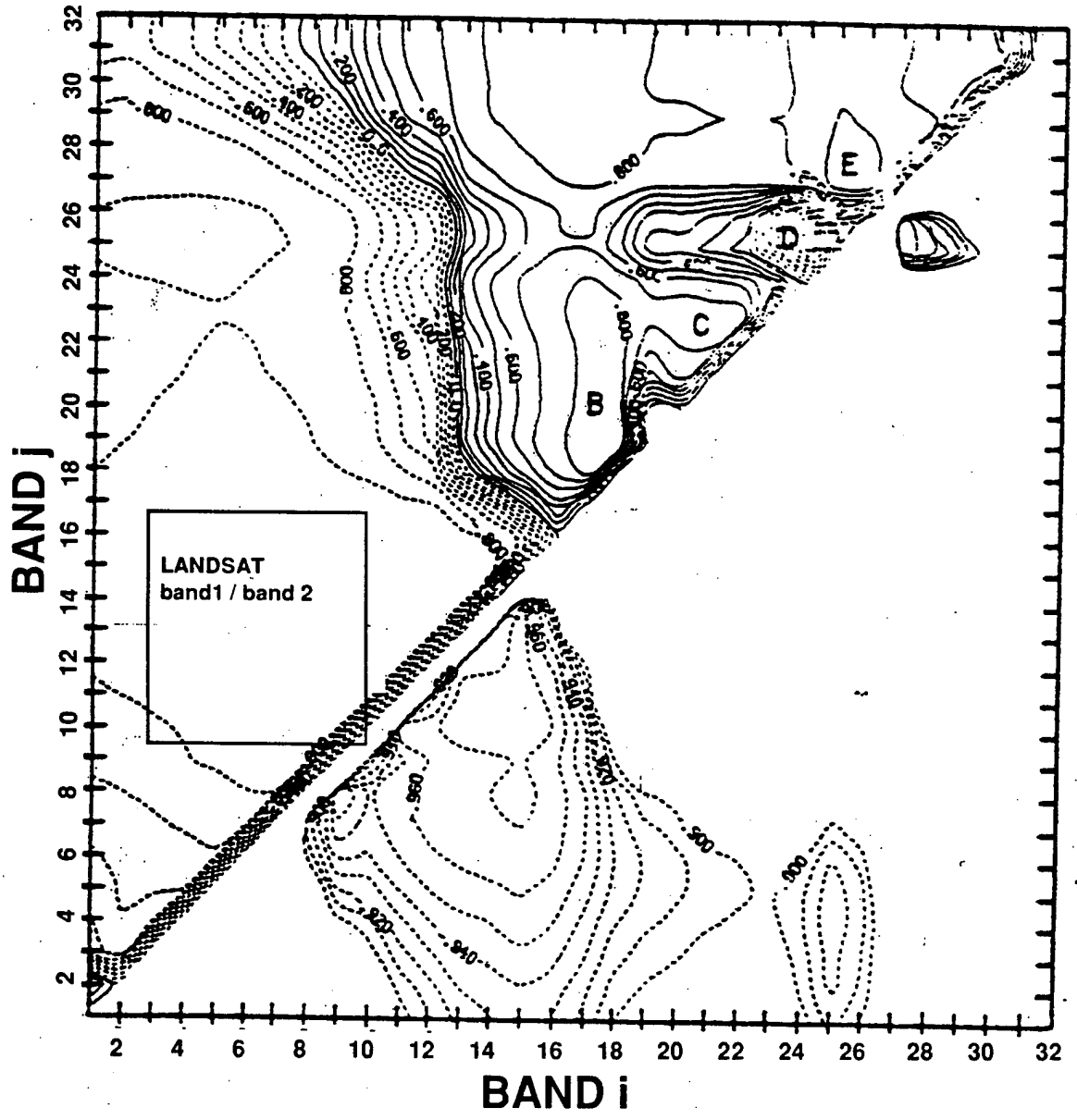

Figure 5-11 Regression Contours for Chlorophyll with Overlay of LANDSAT Bands

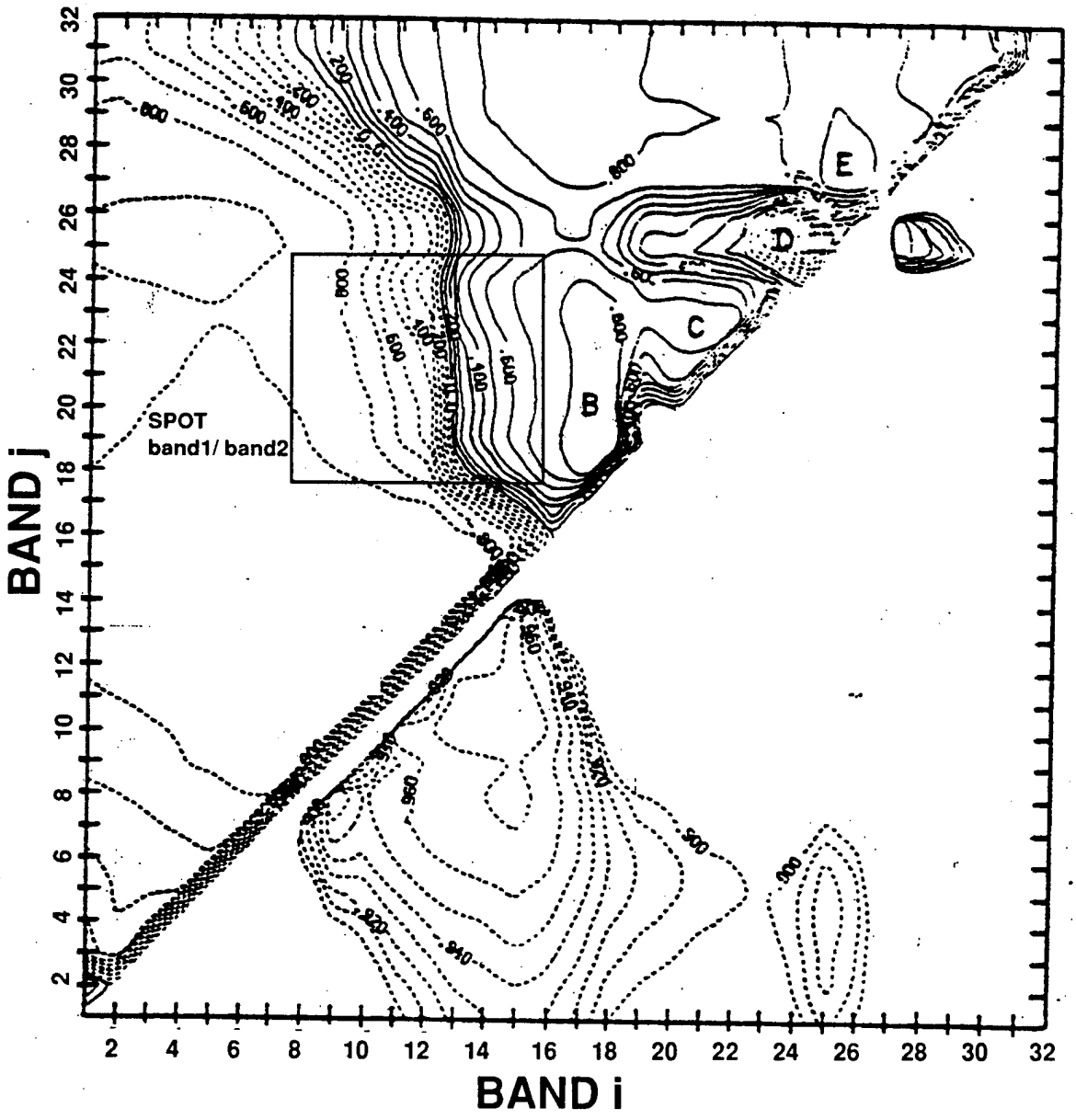

Figure 5-12 Regression Contours for Chlorophyll with Overlay of SPOT Bands

5.3 Summary of Optical Remote Sensing

The chart shown in Figure 5-13 is a summary stop/go matrix chart for the satellite and aircraft sensors and indicates their relative utility for measurement of various physical and optical properties of water. Each element of the matrix chart is scored in one of three ways as follows:

1. Best score = Proven and well established method
2. Medium score = Feasibility shown by experiment or analysis
3. Worst score = Not considered to be feasible.

The columns of the chart indicate the measured ocean water quantities and are organized into physical properties, auxiliary properties and optical properties. The physical properties are chlorophyll concentration, sediment concentration and dissolved organics. The auxiliary properties are temperature and currents. The optical properties are diffuse attenuation coefficient and backscatter coefficient. Each of the water properties is additionally sub-classified as to whether the measurement is being made in ocean water or coastal water, with ocean water being defined as a 1 km horizontal pixel scale size in either Case I or Case II water and coastal water defined as a 30 m horizontal pixel scale size in Case II water. In the case of the active aircraft platform the ocean classification is dropped and a depth classification, defined as the ability to depth resolve the properties in the water column, is added.

The rows of the chart indicate the platform and sensor. The platform is either a satellite or an aircraft, with the aircraft platforms being sub-classified into passive (which implies high altitude operation) and active (which implies low altitude operation). The satellites are LANDSAT/TM, SPOT and SeaWiFS. The passive aircraft sensors are AOL, AVIRIS and HYDICE. The active aircraft sensors are the AOL operated as a fluorescence lidar and the AOL operated as a Brillouin or Doppler lidar.

5.3.1 Proven and Well Established

The techniques and measurements that are proven and well established are indicated by the solid dark regions on the matrix chart of Figure 5-13. These are in three general categories: (1) passive sensing of chlorophyll in the open ocean; (2) laser-induced fluorosensing and Raman scattering (3) and thermal water surface temperature sensing. The specific examples that are cited are the following.

- Satellite sensors on LANDSAT and SeaWiFS for measurement of chlorophyll concentration in Case I water in the open ocean with a 1 km pixel size (pixel averaging required for LANDSAT) [Gordon, 1983; Mueller, 1992].
- Satellite sensors on LANDSAT, SPOT and SeaWiFS for ocean surface temperature measurement [McClain, 1981]. Similar sensors can be used on aircraft with adequate spatial resolution for the coastal zone.
- Aircraft passive sensors (AOL, AVIRIS and HYDICE) for measurement of chlorophyll concentration in Case I water in the open ocean. [Hoge, 1986; Hoge 1987]
- Aircraft active laser sensor (AOL) for lidar fluorosensing with water Raman normalization in coastal case II water with 30 m pixel scale size [Kim, 1973; Bristow, 1981; Hoge, 1982].
- Aircraft active laser sensor (AOL) for diffuse attenuation measurements with water Raman lidar. [Bristow, 1981; Hoge, 1983].

5.3.2 Feasibility Shown Through Experiment or Analysis

The techniques and measurements for which feasibility has been shown, but not yet well established or proven, are indicated on the matrix chart as hatched areas.

- Constituent measurements in Case II waters present a challenge to passive sensors because of the complex radiative transfer interactions caused by a combination of scattering from the suspended matter and absorption by dissolved organics together with the absorption and solar-induced fluorescence of chlorophyll. Two general approaches are indicated: (1) the use of site specific algorithms [Tassan, 1994] or (2) the use of inverse retrieval (factor analysis) techniques [Fischer, 1986; Fischer, 1987; Sathyendranath, 1987]. While some success has been obtained and feasibility has been shown neither approach can yet be considered as proven and well established.
- The use of laser-induced fluorescence in combination with passive ocean color has been shown to enhance the retrieval of ocean water constituents [Sathyendranath, 1994] although the generality of this approach has not yet been developed.
- To the extent that the physical properties can be determined by passive sensors then estimates of diffuse attenuation can be obtained, as was shown by analysis of CZCS data [Austin, 1981].
- Depth resolved water temperature (or sound velocity) measurements have been shown to be feasible with pulsed laser excitation from an aircraft platform by

either Raman [Leonard, 1979] or Brillouin [Leonard, 1988; Hickman, 1992] methods.

- Brillouin lidar measurements have also been shown feasible for depth resolved Doppler measurement of both currents and absolute backscatter coefficients [Leonard, 1988].

5.3.3 Measurements not Currently Feasible

The techniques and measurements remaining as elements on the matrix chart that are deemed not feasible by existing technology are indicated by the circle/slash symbol.

- Measurements with existing satellites of constituent concentrations in Case II water with a 30 m horizontal pixel size are contraindicated due to a lack of sensitivity as discussed in Section 5. During this contract satellite concepts were developed (see Appendices C and D) that combine high sensitivity and small pixel size and that can satisfy the requirements of the coastal water clarity prediction requirements. Aircraft platforms have shown the feasibility of both high sensitivity and adequate spatial resolution.
- Brillouin measurements by their basic nature, can not determine the concentration of water constituents.
- Current are not available from instantaneous passive ocean color measurements or from fluorescence lidar.
- Backscatter coefficients can not be obtained directly from passive measurements since algorithms have not yet been shown to be feasible to retrieve backscatter coefficients from ocean color data.

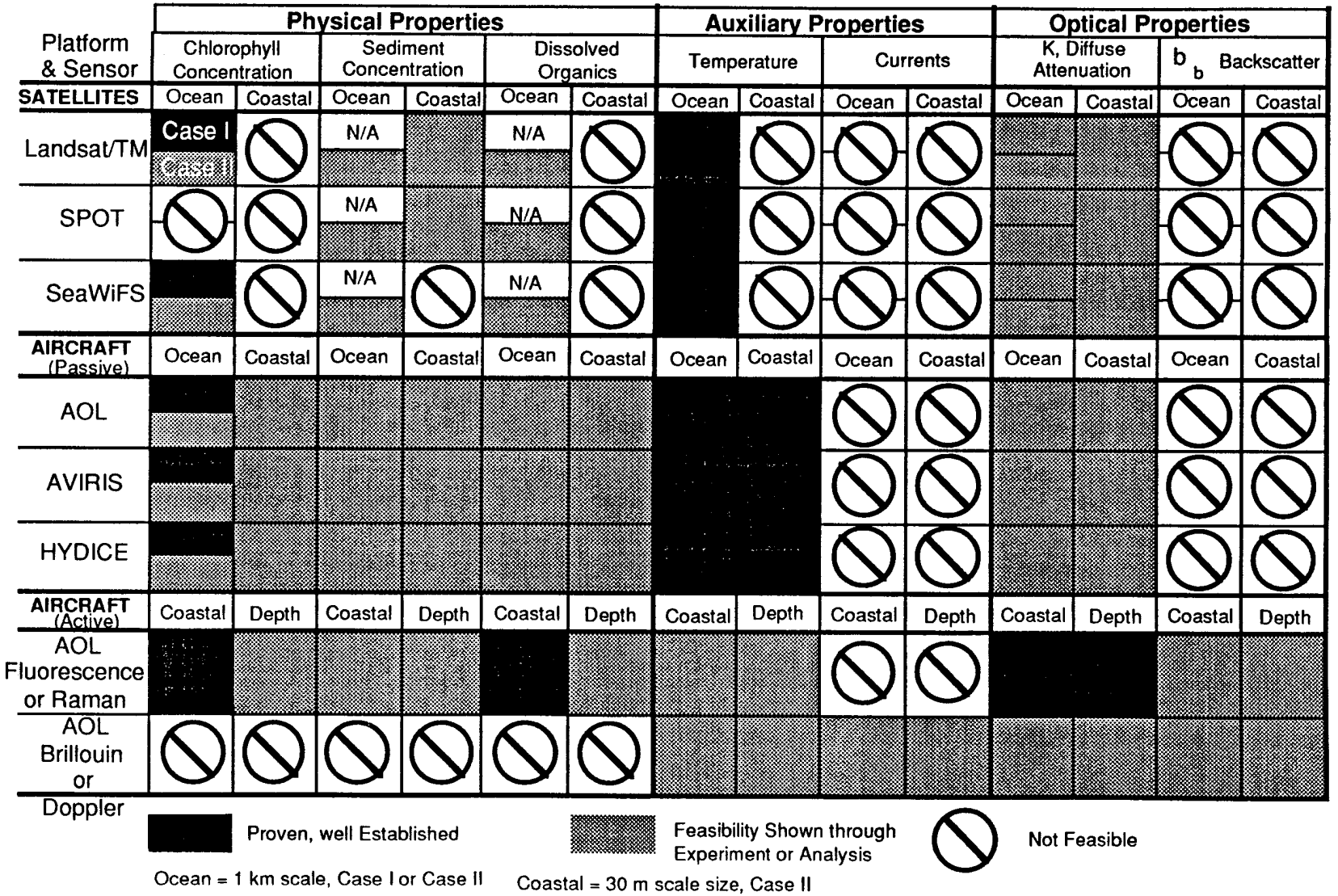

Figure 5-13 Summary Stop/go Matrix Chart for Satellite and Aircraft Sensors

6.0 Remote Sensing Development

Two new concepts were developed to improve the capability of satellite multispectral imaging of coastal zone waters. One concept utilizes a narrow swath sensor array in which longer effective dwell time is achieved by time-delayed integration (TDI). The second concept utilizes a shot-noise limited image intensified array sensor, and the device currently commercially marketed by Xybion is analyzed as an example of such a concept.

6.1 Concepts for Shot-Noise Limited Satellite Multispectral Imaging

Satellite imaging over land is typically done with instruments providing relatively high spatial resolution (10-30 m), moderate spectral resolution (60-140 nm), and moderate SNRs (≈100). Imaging over water requires much higher SNRs, on the order of 500, and narrow spectral bands, 10 - 20 nm. As a consequence of the need for very high SNR and relatively high spectral resolution, while limiting the dimensions of the imaging instrument, ocean color imagers generally have very poor spatial resolution. The CZCS and SeaWiFS, for example, have instantaneous fields of view of 1 km. This is adequate for work in the open ocean, but is much too coarse for observations in the coastal zone, especially along convoluted shorelines.

The technical problem is how to achieve suitably high SNR, and high spectral resolution, along with high spatial resolution, in an instrument of reasonable size. Considering the trend of modern satellite platforms, to ever smaller dimensions compatible with low-cost launch vehicles, "reasonable-size" may mean very small dimensions. Two potential solutions were considered and these are discussed in some detail in Appendix C "Concept for Narrow-Swath Increased Dwell Time Satellite Sensor," and Appendix D "Potential Application with XYBION Camera: Target of Opportunity"

7.0 Conclusions and Recommendations

The following expresses the conclusions derived from the work performed and the recommendations that were developed.

7.1 Operations Concept Development

The integration of coastal water optical quality prediction with the overall Navy operations scenario should be developed so that costs and benefits can be quantified. The complementarity of satellite and aircraft sensors and the fusion with data from other sources such as in situ sensors should be considered. Inclusion of the coastal water prediction capability into the existing Tactical Environmental Simulation System (TESS) for integration with Navy users should be an assumed goal of the overall effort.

7.2 Requirements Definition

Following the operations concept development, a matrix should be developed of critical optical coastal water properties (both range of values and accuracy) vs. operational optics-oriented systems requirements. The result should be the definition of the sensitivity of the system performance prediction to the (required) accuracy of the water properties.

7.3 Operational Reconnaissance Development

The following development of reconnaissance systems is recommended in order to provide critical capabilities that do not now exist.

7.3.1 Dedicated Coastal Zone Satellite Sensor Systems

A narrow swath, small pixel, high signal-to-noise ratio sensor concept, optimized for coastal zone measurement is a mandatory requirement, if satellite sensors are to be successfully used for coastal water optical properties prediction. No current or planned satellite sensor has the necessary capability

It is recommended that proof-of-principle development tasks be initiated on a dedicated coastal water satellite sensor concept, such as is described in Appendix C.

7.3.2 Unmanned Aircraft Coastal Zone Sensor Systems

The emphasis in this area should be the development of small and efficient sensors suitable for use in unmanned reconnaissance aircraft. The combined and simultaneous use of passive and active sensors has been shown to result in an overall sensor

capability with high specificity and accuracy. The unique depth resolved capability of the active sensor is also important. The orientation toward unmanned aircraft would appear to be an essential requirement, but not yet validated by an operations concept for the overall coastal water prediction system.

It is recommended that concept development work be initiated for an unmanned aircraft sensor system that incorporates, to the maximum possible, the attributes of the active and passive aircraft sensors described in Sections 4.3 and 4.4.

7.3.3 Coastal Zone In Situ Sensors

The specific baseline in situ sensor(s) selected will depend greatly on the operational concept that is developed. It is concluded however that in situ sensors that are capable of measurement of the volume scattering function (VSF) should be developed since a capability to measure the VSF by remote sensing from aircraft or satellite remote sensors has not yet been demonstrated. The VSF is an important inherent property which in combination with the absorption coefficient can enable the prediction of underwater imaging. This is especially important under range limited conditions.

Although the need has not yet been validated by a formal operations concept, it is strongly recommended that concept development work be initiated for a VSF measurement capability on unmanned autonomous vehicles.

7.4 Validation Tests of Sensors and Algorithms

The critical issues relating to each measurement should be established and appropriate validation tests defined. Suitable sensors and sensor platforms should be identified for test use.

7.5 Reconnaissance Systems Implementation Plan

A plan should be developed for implementing a coastal water optical properties prediction reconnaissance system. The plan should include the optimum exploitation of existing and planned reconnaissance measurement capabilities, as well as the development of unique and necessary new capabilities.

REFERENCES

Austin, R. W. and T. J. Petzold, "An Instrument for the Measurement of Spectral Attenuation Coefficient and Narrow Angle Volume Scattering Function of Ocean Waters," SPIE 64, Ocean Optics, pg. 50 (1975).

Austin, R. W. and T. J. Petzold, "The Determination of the Diffuse Attenuation Coefficient of Sea Water Using the Coastal Zone Color Scanner," Oceanography from Space, J. Gower, Ed., Plenum Press, New York (1981) pps 239-256.

Austin, R. W. and T. J. Petzold, "Spectral Dependence of the Diffuse Attenuation Coefficient of Light in Ocean Waters," Opt. Eng. 25, 471 (1986).

Bristow, M., "Use of Water Raman Emission to Correct Airborne Laser Fluorosensor Data for Effects of Water Optical Attenuation," Appl. Opt. 20, 2889 (1981).

Browell, E. V., "Analysis of Laser Fluorosensor Systems for Remote Algae Detection and Quantification," NASA Technical Note TN D-8447, NASA, Washington, D.C. (June 1977).

Carder, K. L. et al., "AVIRIS Calibration and Application in Coastal Oceanic Environments," Remote Sens. Environ. 44, 205 (1993)

Doerffer, et al., "Analysis of Thematic Mapper Data for Studying the Suspended Matter Distribution in the Coastal Area of the German Bight (North Sea)," Remote Sens. Environ. 28, 61 (1989).

Ekstrand, S., "Quantification of Chlorophyll a in Coastal Waters Using LANDSAT TM," Remote Sens. of the Environ., Rio de Janeiro, Brazil, May 1991, page 925.

Ekstrand, S., "LANDSAT TM-based Quantification of Chlorophyll-a During Algae Blooms in Coastal Waters," Int. J. Remote Sensing, 13, 1913 (1992).

ER Mapper, Product Information Version 4.0, Earth Resource Mapping Ltd., Suite 900, 4370 La Jolla Village Drive, San Diego, CA 92122

Fischer, J., R. Doerffer and H. Grassl, "Factor Analysis of Multispectral Radiances Over Coastal and Open Ocean Water Based on Radiative Transfer Calculations," Appl. Opt. 25, 448 (1986).

Fischer, J. and R. Doerffer, "An inverse Technique for Remote Detection of Suspended Matter, Phytoplankton and Yellow Substance from CZCS Measurements," Adv. Space. Res. 7, 21 (1987).

Gordon, H. R., "Removal of Atmospheric Effects from Satellite Imagery of Oceans", Appl. Opt. 17, 1631 (1978).

Gordon, H. R., et al., "Phytoplankton Pigment Concentrations in the Middle Atlantic Bight: Comparison of Ship Determinations and CZCS Estimates," Appl. Opt. 22, 20 (1983).

Gordon, H. R. and A. Morel, "Remote Assessment of Ocean Color for Interpretation of Satellite Visible Imagery, a Review," in Lecture Notes on Coastal and Estuarine Studies, ed. Barber et al., Springer-Verlag, New York, 1983.

Hickman, G. D. et al. "Aircraft Laser Sensing of Sound Velocity in Water: Brillouin Scattering," Remote Sens. Environ. 56, 165 (1991).

Hoge, F. E., and Swift, R. N., "Delineation of Estuarine Fronts in the German Bight using Airborne Laser-induced Water Raman Backscatter and Fluorescence of Water Column Constituents," Int. J. of Remote Sensing 3, 475 (1982).

Hoge, F. E., and Swift, R. N., "Airborne Detection of Ocean Turbidity Cell Structure using Depth-resolved Laser-induced water Raman Backscatter," Appl. Opt. 23, 3778 (1983).

Hoge F.E., R. E. Berry and R. N. Swift, "Active-passive Airborne Ocean Color Measurement. 1: Instrumentation," Appl. Opt. 25, 39 (1986).

Hoge, F.E. , C. W. Wright and R. N. Swift, "Radiance-Ratio Algorithm Wavelengths for Remote Oceanic Chlorophyll Determination," Appl. Opt. 26, 2082 (1987).

Holder, Dennis, PE&RS, Volume LVIII, Number 10, October 1992. (See also D. Holder, "Debanding Thematic Mapper Imagery," Ph.D. Dissertation, North Dakota State University, 1990.)

Hooker, S. B., et al., "SeaWiFS Technical Report Series, Volume 1, "An Overview of SeaWiFS and Ocean Color," NASA Technical Memorandum 104566, Vol 1, July 1992.

Horiba Instruments, Inc., Particle Sizing Seminar, Notes and Workbook, August 1992; Horiba Instruments, Inc. 17671 Armstrong Avenue, Irvine, California.

Hovis, W. A., et al., "Nimbus-7 Coastal Zone Colour Scanner: System Description and Initial Imagery," Science 210, 60 (1980).

Jensen, J. R. "Introductory Digital Image Analysis," 1986, pg. 95.

Kim, H., "New Algae Mapping Technique by the Use of an Airborne Laser Fluorosensor," Appl. Opt. 12, 1454 (1973).

Leonard, D. et al., "Remote Sensing of Subsurface Water Temperature by Raman Scattering," Appl. Opt. 18, 1732 (1979).

Leonard, D. and H. Sweeney, "Remote Sensing of Ocean Physical Properties; a Comparison of Raman and Brillouin Techniques," SPIE Ocean Optics IX 25, 407 (1988).

McClain, C., "Multiple Atmospheric-window Techniques for Satellite-derived Sea Surface Temperatures," Oceanography from Space , 1981, page 73.

Mueller, J. L., and Austin, R. W., "SeaWiFS Technical Report Series, Volume 5, "Ocean Optics Protocols for SeaWiFS Validation," NASA Technical Memorandum 104566, Vol 5, 1992.

Mueller, J.L., et al., "SeaWiFS Technical Report Series, Volume 27, "Case Studies for SeaWiFS Calibration and Validation, Part3," NASA Technical Memorandum 104566, Vol 27, May 1995, page 20.

Nichol, J. and A. Gupta, "Remote Sensing of Sediment Plumes in South-East Asia; A Case Study of Singapore," Remote Sensing of the Environment, Bangkok, Thailand, April 1990, pg. 385.

Porter, W. M. and H. T. Enmark, "System Overview of the Airborne Visible/Infrared Imaging Spectrometer (AVIRIS)," Proc. SPIE 834 Imaging Spectroscopy II, (1987) pages 114-126.

Richards, J.A. "Remote Sensing Digital Image Analysis," 1986, pg. 41.

Sathyendranath, S., L. Prieur and A. Morel, "An Evaluation of the Problems of Chlorophyl Retrieval from Ocean Color, for Case 2 Waters," Adv. Space Res. 7, 27 (1987).

Sathyendranath, S., et al., "Detection of Phytoplankton Pigments from Ocean Color: Improved Algorithms," Appl. Opt. 33, 1081 (1994).

Schiller, H. and R. Doerffer, "Fast Computational Scheme for Inverse Modeling of Multi-spectral Radiances; Application for Remote Sensing of the Ocean", Appl. Opt. 32, 3280 (1993).

Sweeney, H., P. Titterton and D. Leonard, "Apparatus for Measuring Diffuse Attenuation of Sea Water," Patent No. 4,986,655 (1991) and "Method of Remotely Measuring Diffuse Attenuation Coefficient of Sea Water," Patent No. 4,986,656 (1991).

Tassan, S., "Local Algorithms using SeaWiFS Data for the Retrieval of Phytoplankton, Pigments, Suspended Sediment, and Yellow Substance in Coastal Waters," Appl. Opt. 33, 2369 (1994).

Tassan, S., "Evaluation of the Potential of the Thematic Mapper for Marine Applications," Int. J. of Remote Sensing, 8, 1455 (1987).

Zimmerman, A.V. et al., "Research and Investigation of the Radiation Induced by a Laser Beam Incident on Sea Water," Contractor Final Report CR-14519, NASA grant NSG-1096, Chesapeake College, Wye Mills, MD. (1976).

APPENDIX A

Date	Place	Event
1/15/93	SAIC / San Diego	Project kick-off meeting. W. Stachnik and D. Johnson representing ONR. Program goals discussed
2/9/93	CHORS / San Diego	Met with J. Cleveland and J. Mueller. Discussed chlorophyll optics, growth rate models and significant initial conditions
4/14/93	SPIE Orlando	Attend technical conference on Aerospace Remote Sensing
6/2/93	SAIC / San Diego	Technical Review
7/29/93	SAIC / San Diego	Technical exchange meeting with SAIC predictive modeling group.
9/3/93	EOO / Sunnyvale	Technical exchange meeting with W. Stachnik of ONR.
10/15/93	ONR Arlington, VA	Technical Program Review meeting with D. Johnson, W. Stachnik and other technical staff of ONR. Requirement for better sensitivity presented. Proj. Hercules suggested as possible means to test increased sensitivity capability.
10/28/93	NVEOL Ft. Belvoir	Technical discussions with C. Simi re: possibility of use of shot noise limited multispectral imager (Xybion) for viewing littoral water as add-on to project Hercules.
11/15/93	NVEOL Ft. Belvoir	Technical discussions with C. Simi re: shot noise limited detection & multispectral imaging
1/94	NASA Ames	Technical discussions with M. Fitzgerald, Ames aircraft data facility. Flys ER-2 (three) and C-130 (one). Data collection only. AVIRIS data analysis done by JPL.
1/28/94	New Orleans	Attended Thematic Mapper Conference. Discussed scattered light limitations of SeaWiFS with SBRC design engineers. Tour of Marine Spill Research Corp. (MSRC) aircraft.
2/16/94	NVEOL Ft. Belvoir	Technical discussions with C. Simi re: shot noise limited detection & multispectral imaging
2/22/94	ER Mapper, Inc.	Technical discussions re: methods of reducing satellite multi-spectral imagery to retrieve physical properties
2/22/94	SAIC / San Diego	Technical Program Review for ONR peer group.
2/23/94	Xybion San Diego	Technical discussion with M. Sartor et al. re: characteristics of imager including SNR and PSF details.
4/21/94	SAIC / San Diego	Technical discussion with R. Hammond re: required initial data for predictive model
6/24/94	SAIC / San Diego	Technical discussion with R. Hammond re: required initial data for predictive model
7/22/94	ONR Arlington, VA	Technical exchange meeting with W. Stachnik of ONR.
8/22/94	NASA / Wallops	Tour of AOL facility and technical discussion with F. Hoge re: current utilization of AOI as Ground truth for satellite remote sensing measurement and availability for Navy utilization for reconnaissance system validation testing.
8/23/94	NASA / Goddard	Technical discussion with C. McClain re: SeaWiFS performance details. Confirmed that internal scattering limits utility within 10 km of shoreline
8/23/94	NASA / Goddard	Technical discussion with J. Barker re: use of LANDSAT over littoral water, including limiting noise sources

United States Patent [19]

Leonard et al.

[11] **Patent Number: 4,907,887**

[45] **Date of Patent: Mar. 13, 1990**

[54] **HIGH RESOLUTION INTERFEROMETER WITH HIGH ETENDUE**

[75] Inventors: **Donald A. Leonard**, Cupertino; **Harold E. Sweeney**, Menlo Park, both of Calif.

[73] Assignee: **GTE Government Systems Corporation**, Stamford, Conn.

[21] Appl. No.: **269,816**

[22] Filed: **Nov. 10, 1988**

[51] **Int. Cl.**[4] **G01B 9/02**

[52] **U.S. Cl.** **356/352**; 356/236

[58] **Field of Search** 356/352, 236; 250/228

[56] **References Cited**

U.S. PATENT DOCUMENTS

3,795,448 3/1974 Fletcher et al. ..... 356/352 X

OTHER PUBLICATIONS

Paul et al., "Rapid Velocity Sensor Using a Static Confocal Fabry-Perot and a Single Frequency Argon Laser", *J. Phys. E*, vol. 4, No. 3, pp. 170-172, 3/71.

Primary Examiner—Davis L. Willis
Assistant Examiner—Matthew W. Koren
Attorney, Agent, or Firm—Douglas M. Gilbert; John F. Lawler

[57] **ABSTRACT**

The etendue (throughput or area-solid angle product) of a high resolution interferometer is maintained at a substantially high level by use of a transparent chamber defined by a highly reflective internal surface, the chamber being located at the input to the interferometer. The chamber has an input aperture to admit light into the chamber and an output aperture or exit opening to pass light to the interferometer. By integrating the input light through multiple reflections thereof within the chamber until it exits to the interferometer, the etendue of the latter is substantially enhanced.

7 Claims, 1 Drawing Sheet

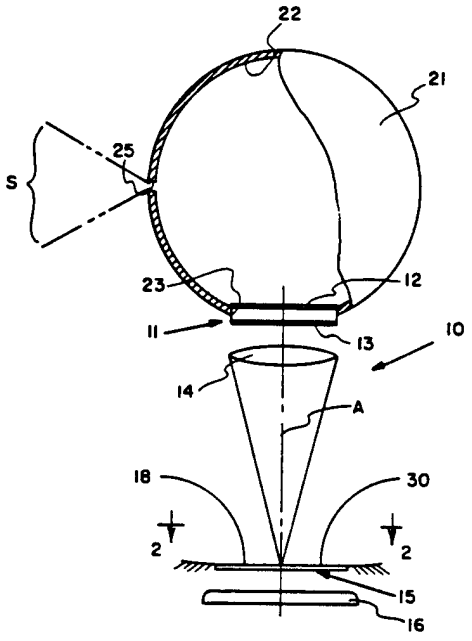

United States Patent [19]

Sweeney et al.

[11] **Patent Number: 4,986,655**

[45] **Date of Patent: Jan. 22, 1991**

[54] **APPARATUS FOR MEASURING DIFFUSE ATTENUATION COEFFICIENT OF SEA WATER**

[75] Inventors: **Harold E. Sweeney**, Menlo Park; **Paul J. Titterton**, Palo Alto; **Donald A. Leonard**, Cupertino, all of Calif.

[73] Assignee: **GTE Government Systems Corporation**, Stamford, Conn.

[21] Appl. No.: **443,620**

[22] Filed: **Nov. 30, 1989**

[51] **Int. Cl.**[5] **G01N 21/00**; G01J 3/44

[52] **U.S. Cl.** **356/73**; 356/301

[58] **Field of Search** 356/301, 43, 73; 250/574

[56] **References Cited**

U.S. PATENT DOCUMENTS

4,123,160	10/1978	Caputo et al.	356/75
4,411,525	10/1983	Ogawa	356/318
4,867,558	9/1989	Leonard et al.	356/349

FOREIGN PATENT DOCUMENTS

2150283A	6/1985	United Kingdom	356/73

OTHER PUBLICATIONS

Atomic Resonance Filters, Gelbwachs, IEEE, 4/29/87, pp. 1266–1277.

Nato Advisory Group for Aerospace Research and Development, Austin et al., 4/10/81, pp. 18–1–18–9.

Iodine Filter in Raman and Brillouin Spectroscopy, Schoen et al., J. Phy. E. Sci. Inst, 6/72, pp. 509–512.

Computer Control of Raman & Brillouin Spectrometers, Rowell et al., Proceedings of the VIIIth International Conference on Raman Spectra., 1980, pp. 444–445.

"Brillouin Scattering in Water: The Landau–Placzek Ratio" by C. L. O'Connor, J. P. Schlept, *Journal of Chemical Physics*, vol. 47, No. 1, Jul. 1, 67, pp. 31–38.

"Atomic Resonance Filters" by J. A. Gelbwachs, *IEEE Journal of Quantum Physics*, vol. 24, No. 7, Jul. 1988, pp. 1266–1277.

"Remote Sensing of the Diffuse Attenuation Coefficient of Ocean Water" by R. W. Austin, *Special Topics in Optical Propagation*, AGARD Conference Proceedings, No. 300, pp. 18–1 and 18–9.

"Spectral Dependence of the Diffuse Attenuation Co—Efficient of Light in Ocean Waters" by R. W. Austin, T. J. Petzoid, *Optical Engineering*, Mar. 1986, vol. 25, No. 3, pp. 471–479.

"Optical Properties of the Clearest Natural Waters (200–800 nm)" by Raymond C. Smith, Karen S. Baker, *Applied Optics*, Jan. 15,1981, vol. 20, No. 2, pp. 177–184.

Primary Examiner—F. L. Evans

Assistant Examiner—K. P. Hantis

Attorney, Agent, or Firm—Douglas M. Gilbert; John F. Lawler

[57] **ABSTRACT**

Apparatus is disclosed for remotely measuring the diffuse attenuation coefficient K of ocean water from a platform such as an aircraft flying over the ocean. A pulsed laser beam is directed as a probe beam from the aircraft into the water to produce therein Brillouin backscattering signals which emanate back up through the water to the aircraft. An optical receiver in the aircraft receives and processes those backscattered signals. A very narrow optical bandpass filter passes the Brillouin signals to a photodetector, a digitizer and a data processor, the latter being programmed to compute the diffuse attenuation coefficient at predetermined depths and at the Brillouin wavelength. Measurements of the diffuse attenuation coefficient at various depths is accomplished by sampling and digitizing the Brillouin signals at predetermined intervals, each interval corresponding to a depth beneath the surface of the water. A preferred embodiment of the invention features similar apparatus having two signal-processing channels for simultaneously deriving the diffuse attenuation coefficient at two wavelengths by analyzing the upwelling Brillouin (blue) and Raman (green) backscatter generated by the probe beam. An alternate embodiment of the invention features apparatus for measuring the diffuse attenuation coefficient K of ocean water from a submerged submarine.

16 Claims, 7 Drawing Sheets

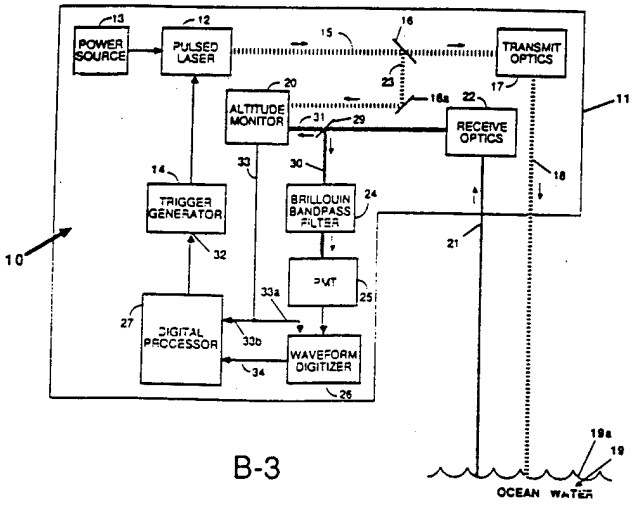

United States Patent [19]

Sweeney et al.

[11] **Patent Number: 4,986,656**

[45] **Date of Patent: Jan. 22, 1991**

[54] **METHOD OF REMOTELY MEASURING DIFFUSE ATTENUATION COEFFICIENT OF SEA WATER**

[75] Inventors: **Harold E. Sweeney**, Menlo Park; **Paul J. Titterton**, Palo Alto; **Donald A. Leonard**, Cupertino, all of Calif.

[73] Assignee: **GTE Government Systems Corporation**, Stamford, Conn.

[21] Appl. No.: **443,679**

[22] Filed: **Nov. 30, 1989**

[51] **Int. Cl.**[5] **G01N 21/00; G01J 3/44**

[52] **U.S. Cl.** **356/73; 356/301**

[58] **Field of Search** 356/301, 43, 73; 250/574

[56] **References Cited**

U.S. PATENT DOCUMENTS

4,123,160	10/1978	Caputo et al.	356/75
4,411,525	10/1983	Ogawa	356/318
4,853,543	8/1989	Ozdemir	356/51
4,867,558	9/1989	Leonard et al.	356/349

FOREIGN PATENT DOCUMENTS

2150283A	6/1985	United Kingdom	356/73

OTHER PUBLICATIONS

NATO Advisory Group for Aerospace Research and Development, Austin et al., 41081, pp. 18-1-18-9.

"Brillouin Scattering in Water: The Landau-Placzek Ratio" by C. L. O'Conner, J. P. Schlept, *Journal of Chemical Physics*, vol. 47, No. 1, 1 Jul. 67, pp. 31-38.

"Atomic Resonance Filters" by J. A. Gelbwachs, *IEEE Journal of Quantum Physics*, vol. 24, No. 7, Jul. 1988, pp. 1266-1277.

"Remote Sensing of the Diffuse Attenuation Coefficient of Ocean Water" by R. W. Austin, *Special Topics in Optical Propagation*, AGARD Conference Proceedings No. 300, pp. 18-1-18-9.

"Spectral Dependence of the Diffuse Attenuation Co-Efficient of Light in Ocean Waters" by R. W. Austin, T. J. Petzoid, *Optical Engineering*, Mar. 1986, vol. 25 No. 3, pp. 471-479.

"Optical Properties of the Clearest Natural Waters (200-800 nm)" by Raymond C. Smith, Karen S. Baker, *Applied Optics*, 15 Jan. 1981, Bol. 20, No. 2, pp. 177-184.

Primary Examiner—F. L. Evans
Assistant Examiner—K. P. Hantis
Attorney, Agent, or Firm—Douglas M. Gilbert; John F. Lawler

[57] **ABSTRACT**

A method of remotely measuring the diffuse attenuation coefficient K of ocean water from an airborne platform such as an aircraft. By directing a pulsed laser beam having a wavelength λ_0 from the platform into the water, the beam interacts therewith to produce inelastic Brillouin backscatter signals at the wavelength λ_1, where $\lambda_1 \neq \lambda_0$. The desired backscatter propagate generally oppositely to the direction of propagation of the pulsed laser beam so that the backscatter can be received and collected at the platform. The upwelling optical energy includes the desired backscatter signals, which are separated out from the remainder of the upwelling optical energy. The separated backscatter signals are converted to equivalent electrical signals and periodically analyzed to generate therefrom the diffuse attenuation coefficient of the ocean water at the λ_1 wavelength at periodic depths beneath the water surface. In another aspect of this invention both the Brillouin backscatter signals and the Raman backscatteer signals are separately filtered out to simultaneously measure the diffuse attenuation coefficient of the water at two distinct wavelengths. In another aspect of this invention the diffused attenation coefficient K is measured from a submerged platform, such as a submarine. This has the advantage of allowing deep ocean layers to be measured along with ocean water beneath the polar ice cap.

9 Claims, 7 Drawing Sheets

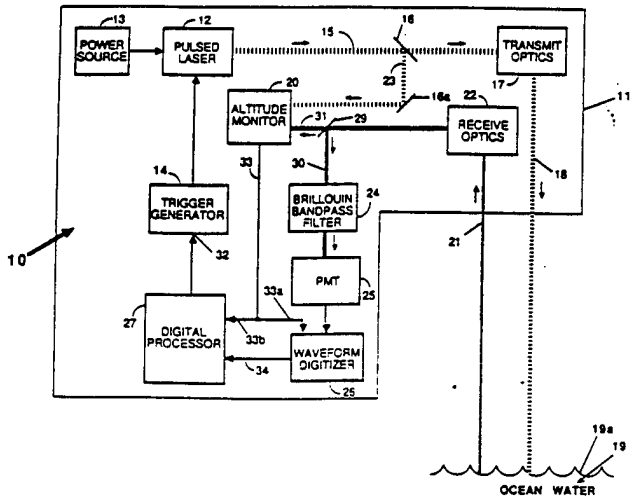

Appendix C

Concept for Narrow-Swath Increased Dwell Time Satellite Sensor

The currently available satellite multispectral imaging sensors do not have the required high sensitivity and small pixel size to be useful in a littoral water reconnaissance sensor. What is needed is an imaging sensor that would have the spatial resolution of a LANDSAT with the sensitivity of a SeaWiFS. We have explored the possibility of a sensor that operates with a narrow directable swath and has a longer effective dwell time per pixel. The following considers the relevant scaling relations for such an imager having both high sensitivity and high resolution, and describes a conceptual design.

C.1 General Scaling of Satellite Imaging Sensors

Consider a satellite imaging sensor detector array of N_X pixels by N_Y pixels that instantaneously views a given area of the ocean. It is apparent that the instantaneously viewed area divided by the rate of area coverage is equal to the dwell time. This can be written as

$$\text{Dwell Time} = \frac{N_x N_y A_p}{V_x (SW)}$$

where

N_X = number of pixels in satellite scan direction
N_Y = number of pixels transverse to satellite scan direction
A_p = area of one pixel (on ocean)
x_p = pixel dimension on ocean (If square pixel $(x_p)^2 = A_p$)
V_X = satellite velocity
SW = swath width

At least two modes of operation can be conceived which are described below.

Mode (1)

A linear array of pixels is scanned transverse to the direction of satellite motion. This is the mode that LANDSAT and SPOT use and is illustrated in Figure C-1. For Mode 1 the lateral scan time equals the satellite transit time across the linear array in the direction of motion thus permitting continuous coverage of the pixels.

$$\text{This scan time is} = \frac{N_x x_p}{V_x}$$

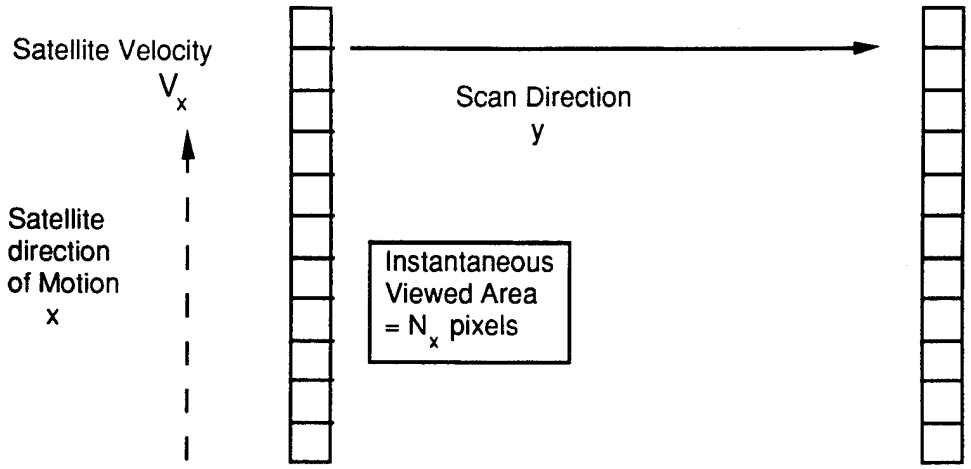

Figure C-1 Mode 1 - Linear Array, Transversely Scanned

Mode (2)

A rectangular array is operated in a stare and step sequence. This mode of operation is illustrated in Figure C-2. In between steps, the scan rate is set to compensate for the movement of the satellite, and thus produce a sequence of "stares" that results in a complete image swath.

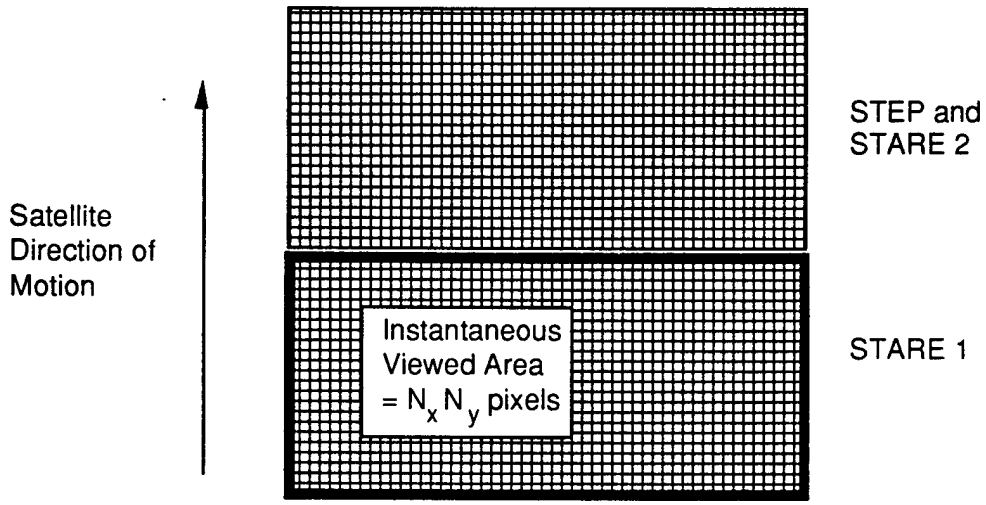

Figure C-2 Mode 2- Rectangular Array, Step and Stare

Note: A superior Mode 2 approach is the use of a time delayed integration (TDI) CCD, rather than a mechanical step and stare. The superiority of this approach is especially valid for satellite operation where low reliability of mechanical devices and problems of angular momentum and vibration coupling are problems best avoided. A TDI CCD is a two-dimensional array in which the rows can be clocked sequentially along the flight

direction, and synchronized such that the illumination from any one ground location follows the charge packet as it ripples down the CCD column.

The stare time for Mode 2 is = $\frac{N_x x_p}{V_x}$, which is equal to the scan time for Mode 1.

The number of photons collected by a detector in either mode is proportional to the dwell time of the detector (assuming other system parameters are kept constant, i.e., QE, aperture, optical efficiency, etc.)

In the case of a satellite as shown above for either mode

$$\text{Dwell time} = \frac{N_x N_y A_p}{V_x (SW)} \qquad = \qquad \left(\frac{A_p}{V_x}\right)\frac{N_x N_y}{SW}$$

which as shown can be broken into two terms; the first relating to the pixel area and the satellite velocity and the second relating to the number of sensor pixels and the swath width. Examining the second term the scaling is quite clear. The number of photons collected is proportional to the total number of pixels and inversely to the swath width.

The following looks at the second term of the dwell time as a figure of merit

$$\text{FOM} = \frac{N_x N_y}{SW} \text{ km}^{-1}$$

<u>For a Mode (1) case, i.e. LANDSAT or SPOT</u>

Typical values are: $N_X = 32$; $N_y = 1$; SW ≈ 100 km

FOM = 32 x 1 / 100 = 0.32 km^{-1}

<u>For a Mode (2) case with a nominal 256 x 1024 pixel array (see following conceptual design discussion)</u>

The corresponding values (for a 20 m pixel size on the water) would be

N_X =256; N_y = 1024; SW = 1024 x 0.02 ≈ 20km

FOM = 256 x 1024 / 20 = 13,107 km^{-1}

Thus the potential improvement from the above Mode (1) example to the Mode (2) example is a factor of

$$13107 / 0.32 = 40{,}960$$

This factor is the relative increase in the number of photoelectrons that each pixel has detected. The improvement in SNR, for a shot noise limited situation, would be the square root of this number, or

$$\text{SNR increases by a factor of } (40{,}960)^{0.5} = 202$$

However since SPOT and LANDSAT are currently instrument limited this SNR improvement factor can not be directly applied. The following details the performance of a Mode (2) array sensor device.

C.2 Conceptual Design of High Sensitivity High Resolution Imager

The following is a design for an ocean color imager, with high sensitivity and high-resolution, based on a TDI CCD. Consider an expression for the signal count rate at an imager detector pixel:

$$N_{pe} = L_o\left(A_{pix}\right)(\delta\lambda)\left(\frac{1}{F^2}\right)T_{opt}Q_{det}\left(\frac{\lambda}{hc}\right)\delta t$$

where

N_{pe}	=	photons counted per pixel
L_o	=	source spectral radiance, W/m^2-μm-sr
A_{det}	=	detector area (one spectral band),
$\delta\lambda$	=	spectral bandwidth, nm
F	=	f/# of receiver optics.
T_{opt}	=	optics efficiency
Q_{det}	=	detector quantum efficiency
λ	=	wavelength
h	=	Plank's constant
c	=	speed of light
δt	=	pixel integration time

The time available for reading one pixel, i.e., δt the pixel integration time, is the Mode (2) stare time which is equal to $\frac{N_x x_p}{V_x}$

Note that one has control over very few of these parameters. Certainly the optical efficiency is always to be maximized. The f/# is limited to a reasonable values near ≈ 2. The detector selection specifies the quantum efficiency. The swath width, pixel field of view, and ground speed are generally fixed by system requirements. Then only the detector area is a free parameter.

The above equation can thus be used to determine what the detector area must be in order to achieve a specified signal to noise ratio. In this regime of very high SNR requirements and visible spectrum wavelengths, the governing parameter is usually the shot noise of the signal, i.e. the square root of the number of photoelectrons detected in each measurement time. The resulting expression for the SNR as a function of detector area is the following

$$SNR = \sqrt{N_{pe}} = \sqrt{A_{pix}} \sqrt{L_o(\delta\lambda)\left(\frac{1}{F^2}\right)T_{opt}Q_{det}\left(\frac{\lambda}{hc}\right)\delta t}$$

Table C-1 shows the shot noise versus single pixel detector diameter for the following parameters, chosen as suitable design values for a small satellite instrument.

λ = 443 nm (the most difficult SeaWiFS band)
L_o = 8.41 mW/cm^2-nm-sr (input radiance for SeaWiFS 443 nm band)
$\delta\lambda$ = 20 nm (as for SeaWiFS)
F = 2.8 (reasonable engineering design point)
T_{opt} = 0.35 (very dependent on optical configuration)
Q_{det} = 0.10 (two dimensional CCD, front-side illuminated)
N_x = 256 (number of pixels in satellite scan direction
x_p = 20 m (the mid range of the desired operating region)
V_x = 7.0 km/s (low orbit, 550 km altitude)
sw = 30 km (1000 cross track pixels)

Table C-1 also shows for each value of SNR the number of photoelectrons collected, the area of the detector array and the diameter of the collection aperture.

Table C-1 Receiver Parameters as Function of SNR

SNR	Single Pixel Detector Diam.	Number of Photoelectrons	Area of Det. Array	Diameter of Collection Optic
1000	9.0 μm	1000000	21.3 mm^2	88 mm
500	4.5	250000	5.3	44
250	2.25	62500	1.33	22
100	0.9	10000	0.21	8.8

Detector Selection

The approach concept suggested for development is a time delayed integration (TDI) CCD. A TDI CCD is a two-dimensional array in which the rows can be clocked sequentially along the flight direction, such that the illumination from any one ground location follows the charge packet as it ripples down the CCD column. The effect is to increase the effective integration time for a single CCD pixel by the number of rows in the CCD. This multiplier ranges from 32 to 256 for currently available TDI CCDs. Such devices have not heretofore seen use in satellite imagers. TDI has been implemented with discrete detectors, as in the Landsat Thematic Mapper and the SeaWiFS. This is limited to a few TDI rows, four in the case of SeaWiFS.

A limitation with the use of TDI is the variation in synchronization speed across the swath. The TDI clocking speed must be equal to the instantaneous field of view (ifov) divided by the ground speed. Far away from nadir the ifov increases due to the greater range, so a TDI array synchronized at nadir will have a clocking error away from nadir. The cumulative clocking error down the TDI column must not be greater than the equivalent of a small fraction of one pixel if the image is not to be severely degraded.

This has prevented the use of large TDI arrays for wide-swath imaging instruments. However, the high resolution littoral zone imager will have a relatively narrow swath, on the order of 20 to 30 km. With such a narrow swath the variation in TDI timing across the swath is negligible.

A suitable detector for this application, selected from currently available units (custom devices can, of course, be obtained without inordinate expense), is the Thomson-CSF TH7885M, with 256 rows of 1024 pixels. This has several characteristics ideal for this application:

- MPP mode operation, for extremely low noise and ionizing radiation tolerance;
- very low dark signal, 0.3 electrons/pixel at the normal operating temperature of -40 degrees C;
- relatively large pixels, 19 μm square, with 100% aperture.

The total effective area of this device is 95 mm^2, so it well exceeds the collection area indicated by the calculations just above. One limitation of this device, and of CCDs in general, is the limited pixel well depth, in this case $4x10^5$ electrons. The SNR goal of =1000:1 corresponds to 10^6 electrons. Implementation of this CCD therefore requires splitting the signal equally between two devices, and limiting the signal to remain below

saturation. Then the practical limit to the shot noise SNR is on the order of 775:1, allowing 25% headroom to the CCD well.

Imager Design

A preliminary conceptual design has been worked out around this detector. The littoral zone imager will have 8 pairs of these detectors, each pair mated with an interference filter for the appropriate band. (Note that interference filters for precision applications must be the newest generation of refractory metal oxide types, prepared with ion assisted deposition to achieve unity fill factors.) For an ifov of each pixel of 20 m, and consequently a swath of 20 km, from an altitude of 550 km, the optics effective focal length will be 523 mm. The aperture will be 186 mm in diameter with f / # 2.8 optics.

These optical parameters are small enough that the imaging instrument can employ multiple optical collectors. The design requirements for each optic can be ameliorated by dividing the spectral channels into the short-wave and long-wave ranges, and requiring each optic to be achromatic only over its relatively limited spectral range.

The use of refractors rather than reflectors eases the problem of achieving a flat field over the full area of the detector (4.9 x 19.5 mm). The angular field of view defined by the swath ($\pm$ 1.6^{o}) is not very large, and the imaging performance (54 μradians, several times the aperture diffraction limit) is not very demanding, so this optical design does not appear to be especially difficult.

Degradation of the SNR by CCD dark current and the support electronics will be very small. The dark current of 0.3 electrons/pixel-second amounts to less than one electron at the TDI readout. The readout noise of 4 electrons is negligible for a signal amounting to 2.8×10^5 electrons. Consequently, the SNR for each band will be on the order of 750:1, which matches the performance of instruments such as the SeaWiFS. The shot noise SNRs for all SeaWiFS bands are in the table following, with the single-detector SNRs tabulated and the paired-detector SNRs in parentheses. The CCD will be clocked at a rate corresponding to the pixel transit time, or 4.3 ms/row. The readout of 1024 pixels between each row clocking is a data rate of 2.4×10^5 pixels/second.

Digitization with sufficient precision that the 530:1 single detector SNR is not degraded requires a minimum of 10 bits. The system data rate, for eight bands, with the paired detectors summed after digitization, is a minimum of 18 Mbps, with full bit

packing. Data storage and telemetry for this system will be challenging. Lossless data compression will yield a factor of 2 to 4 reduction in the data rate.

Small Satellite Implementation

Two optical systems as described above, namely refractors with effective focal length 523 mm and aperture 186 mm, will be packaged as a co-aligned pair. One refractor will be optimized for 400 - 520 nm, and the other for 885 - 565 nm. Each refractor's image will be divided with a three-stage cascade splitter to illuminate eight detectors, or four pairs of two. The last splitter will be preceded by an interference filter to define each passband.

Some rough estimates for the parameters of this instrument are as follows:

Overall dimensions: 30 x30 x 40 cm
Mass: 30 kg
Power requirement: 60 W
Data rate: 10 Mbps

C.3 Pixel Distortion Assessment using TDI

The possible pixel distortion that can occur when using time delayed integration (TDI) is illustrated in Figure C-3. The left hand side is a perfect projection of the array's pixellated field of regard while the right hand side is a rough sketch of the distortion due to the greater distances to the edges of the projection from the sensor positioned at the center of the array projection.

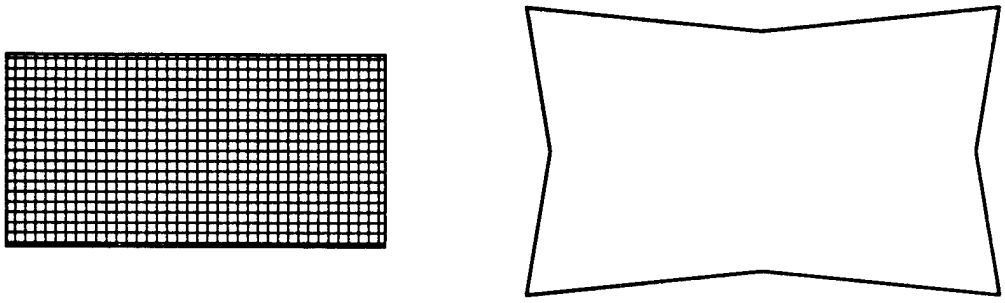

Figure C-3. Illustration of the distortion in the perfect pixel projection due to the distance from the sensor to the surface, for the sensor at the center of the projection.

For the scale of the coastal sampling situation, with the total field of regard of order tens of kilometers, this pixel growth with off-nadir angle, and the concomitant mistiming in the TDI approach is negligible. This can be seen be considering the round earth and

flat earth geometries in Figure C-4, where we have assumed that the sensor subtends the same pixel angles at all nadir angles.

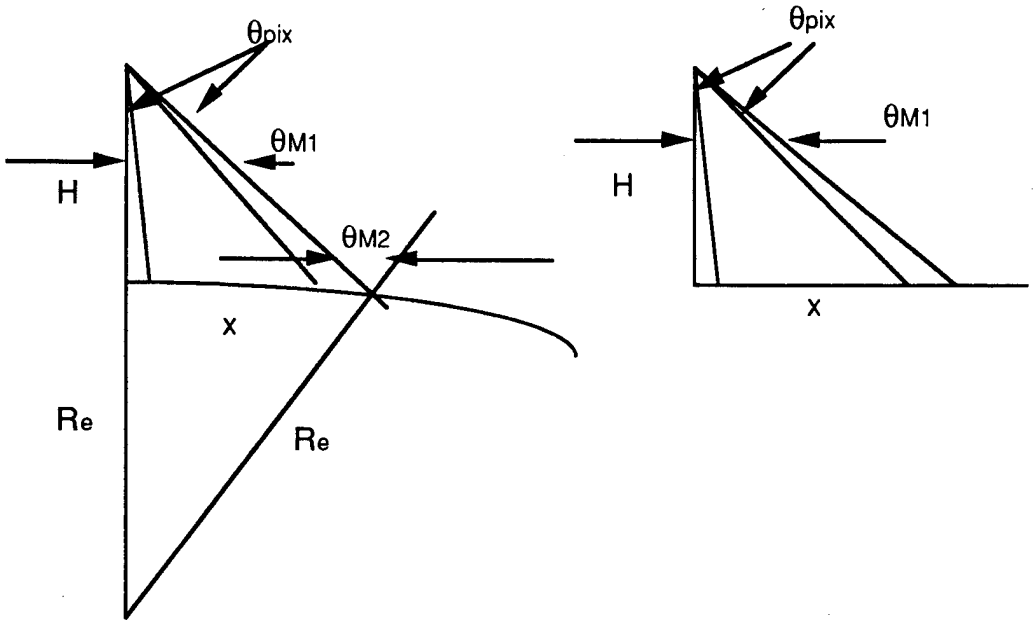

Figure C-4 Round earth and flat earth geometries from the sensor at array center to the center of the edge of the projection.

where

H = satellite altitude
x = distance along the earth
θ_{pix} = pixel angular dimension,
θ_{M1} = half total angular field of regard in satellite-centered co-ordinates,
θ_{M2} = off-zenith line of sight angle for round earth co-ordinates (and evidently in the flat earth case the two values of theta are identical, being alternate interior angles of parallel lines).

We take the reasonable case of the pixel angular dimension determined by the requirement to sense a 20 meter pixel at nadir. For a satellite altitude of 750 km, this implies

$$\theta_{pix} = \frac{20}{H} = 0.001527887^\circ = 26.67 \mu rad .$$

For a rectangular array of 256 x 1024 elements, and the satellite/sensor centered on the field of regard, the total (half-angle) field of regard in the wide direction is given by

$$\theta_{M1} = 512\theta_{pix} = 0.78227838°.$$

In the round earth case, $\theta_{M2} = \sin^{-1}\left(\frac{R_e + H}{R_e}\sin\theta_{M1}\right) = 0.87436123°,$

and

$$x = R_e(\theta_{M2} - \theta_{M1}) = 10{,}240.75 \text{ meters.}$$

For the flat earth (which is expected to give pretty much the same answer because of the small angles involved)

$$x = 750{,}000\tan\theta_{M1} = 10{,}240.64 \text{ meters.}$$

These answers only differ by 11 cm, and since for the perfect pixel projection the x dimension would be 512 x 20 = 10,240 meters, the distortion at the midpoint of the side of the projection is only 75 cm total.

In the forward direction the effect is about 4x smaller, since only 128 pixels are being viewed there, instead of 4 x 128 = 512. Using the flat earth analysis for ease of computation, the y dimension to the center of the top of the projection = 2560.01 meters, which is only 1 cm greater than the perfect pixel projection of 128 x 20 = 2560 meters.

The worst case will be the corner pixel, since it will have the compounded effect of both the lateral and forward distortions. Using the flat earth level of analysis, it is straightforward to find that the x dimension at the corner has grown by only 6 cm while the y dimension has grown by 24 cm. These estimates are summarized in Table C-2.

Table C-2. Total field of regard distortion for a fixed angle per pixel, with a 20 meter pixel at nadir and the sensor at 750 km

Perfect Pixel Projection	Flat Earth projection to Center of side	Flat Earth Projection to corner
Along Track: y=2560 m	2560.01 m	2560.25 m
Cross track: x=10,240 m	10240.64 m	10,240.70 m

All these distortion are negligible compared to the pixel size of 20 meters, and so we can neglect this effect in this application.

Appendix D

Potential Application with XYBION Camera: Target-Of-Opportunity

D.1 Introduction and Summary

We explored the possibility of using a XYBION detector/camera, to be flown on the space shuttle by a tri-service group under the Hercules project, to perform initial proof-of-principle tests for a shot noise limited array satellite sensor. The XYBION device was initially considered to be available for CWC usage tests at minimal cost.

The XYBION is an image intensified device, consisting of a rotating filter wheel, image tube with a photo-cathode and micro-channel-plate image intensifier, an output phosphor, and a fiber-optic relay onto a CCD. The net result is a device with signal shot-noise limited operation that can view each of twelve wavelengths and resolve the scene into ~ 750 x 450 pixels, with a time resolution of ~ 4 milliseconds.

We considered the wavelength set shown in Table D-1.

Table D-1 Optimum Wavelengths Sampled by a CWC Satellite Remote Sensor

Band	λ (nm)	$\Delta\lambda$ (nm)	Justification	Purpose
1	445	20	CZCS, SeaWiFS, Ref. 1	Same as Previous/Planned Sensors
2	490	20	SeaWiFS	Same as Planned Sensor
3	520	20	CZCS/SeaWiFS; Ref. 1, 2	Sample on slope of Reflectivity Peak
4	565	20	TM Band 2; SeaWiFS, Refs. 1, 2	Sediment; Sample on Reflectivity Peak
5	600	20	Ref. 2	Shape of Reflectivity Peak
6	630	10	Ref. 2	Low Reflectivity; cyano
7	640	10	Ref. 1	See reference
8	650	10	Ref. 2	Models low reflectivity Chlorophyll
9	665*	10	Chlorophyll a	Chlorophyll a Absorption
10	685*	10	Chlorophyll a	Chlorophyll a Fluorescence
11	750*	10	SeaWiFS	Atmospheric Radiance Correction
12	865*	10	SeaWiFS	Atmospheric Radiance Correction

References:
1. Sathyendranath, Prieur and Morel, Advanced Space Research, Volume 7 (2), pps. 27 - 30, 1987.
2. Dekker, Malthus and Wijnen 1st Thematic Conference on Remote Sensing for Marine and Coastal Environments, New Orleans, 1992, p. 955.

The XYBION cathode is available in numerous implementations, which provide the responsivities shown in Figure D-1. The GEN III Blue response and the 12 bands cited in Table D-1 have an excellent overlap.

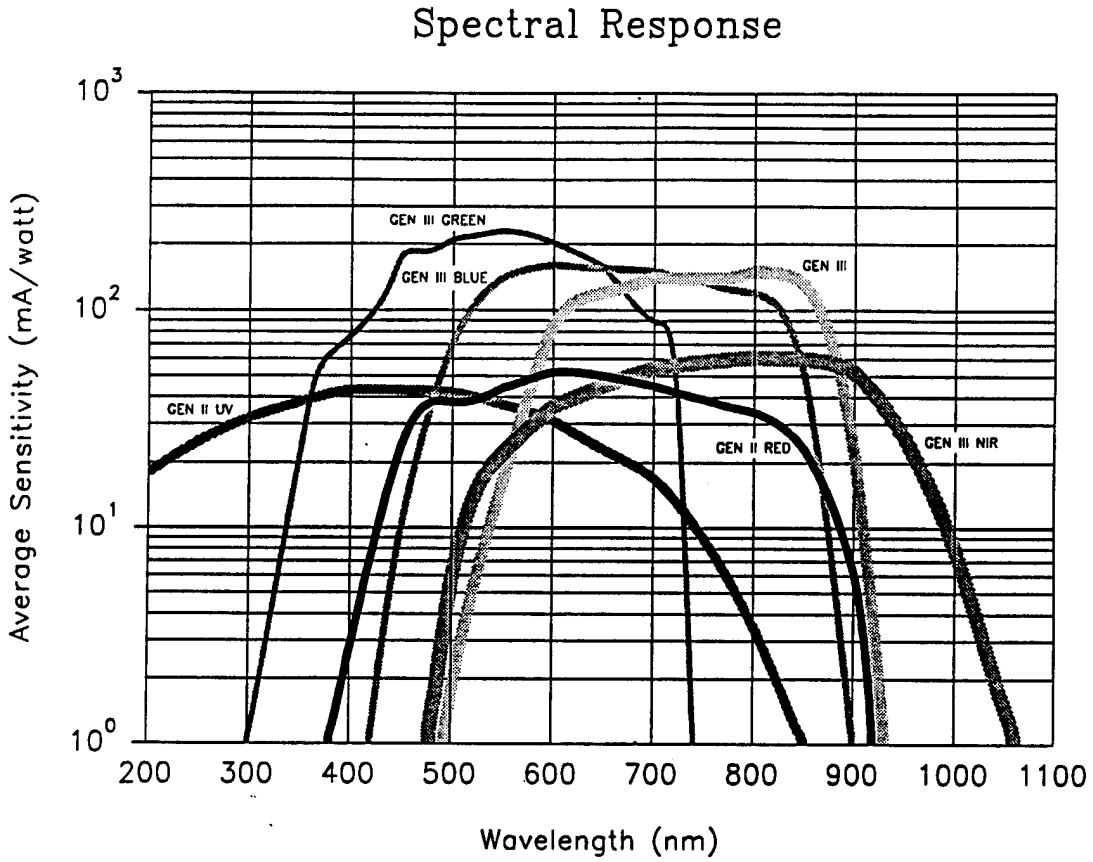

Figure D-1 Available Cathode Responsivities for the XYBION Cameras

As the analysis of a point design for this opportunity proceeded, it became clear that the camera must stop and stare during its progression across any littoral scene. The sub-shuttle spot is moving at approximately 7.4 km/sec along the surface of the earth. In order to collect sufficient signal from pixels of order 10 to 30 meters in extent, the camera must stare at each location for an extended time (as derived below, an exposure of ~ 160 milliseconds is required to obtain an adequate SNR -- a fixed shuttle field of regard moves 20 meters in 2.7 milliseconds). This step and stare approach is feasible if the step is smaller than the overall field of regard of the camera (so there are no gaps between consecutive steps), and if the camera can be reliably pointed during the staring interval. This last requirement is the critical performance cost issue which finally militated against implementation of the opportunity, since it requires pointing to ~ (20 m) ÷ (300,000 m) = 67 μradians during an ~ 100 millisecond stare interval, well

beyond any hand-held-by-astronaut capability, and entailing costly definition, design and implementation of a motion compensation platform.

Nevertheless, we include the analysis for the step and stare device as an example of the scope of the littoral zone remote sensing that can be accomplished with a signal shot noise limited detector and significant dwell time per pixel.

For a shuttle-borne XYBION camera that stares at a fixed location during the exposure time of an individual pixel, the following parameters describe a viable and consistent system:

Shuttle Altitude:	300 km
Optical Aperture Diameter:	15 cm (6 inches)
Optical Transmission:	50%
f# :	1.72
Exposure Time:	158 milli-seconds
Resolution Element:	20 m

The signal levels and (assumed) signal shot noise limited signal to noise ratio for the maximum number of channels (with bandwidths as shown) for the Gordon-radiance levels are shown in Table D-2

Table D-2 Performance of Staring XYBION Camera from Shuttle Altitudes

Band or Channel	Wavelength (nm)	Channel Bandwidth (nm)	Signal Photo-electrons per pixel per exposure time (of 158 milliseconds)	Signal-to-Noise Ratio
1	445	20	278,412	528
2	490	20	1,220,076	1105
3	520	20	1,783,188	1335
4	565	20	2,033,460	1426
5	600	20	1,720,620	1312
6	630	10	675,354	822
7	640	10	628,680	791
8	650	10	563,112	750
9	665	10	531,328	729
10	685	10	491,159	701
11	750	10	297,198	545
12	865	10	68,825	262

D.2 Analysis

The analysis that leads to the above conclusions has three portions:

1. Calculation of the signal level at an individual pixel during a single time exposure, assuming that no smearing occurs -- i.e., that the camera stares at the resolution element during the full exposure time. The key output of this analysis is the [exposure time]$^{1/2}$ x (receiver aperture diameter) x (resolution element size) product required to provide the sensitivity in the channel with the least signal.

2. Top level optical design analysis, relating the optical aperture diameter, equivalent f# of the receiver optical system, and the XYBION camera pixel size to the shuttle-to-surface range and resolution element size. The key output of this analysis is the (receiver aperture diameter) x (resolution element size) x (f#) product for the XYBION camera pixel size and the shuttle altitude.

3. Consistency calculations for the above two analyses, leading to the practical values of receiver aperture diameter for reasonable values of the f# and for the range of resolution element sizes desired for Coastal Water Clarity usage. We also estimate the resulting SNR performance of the sensor in all twelve wavelength bands.

D.2.1 Signal Level:

The average signal power incident on the first photo-cathode of the shuttle-borne camera is given by

$$P_{av} = L_{sig}\left(\frac{\pi D_0^2}{4}\right)\Delta\lambda\left(\frac{A_{RES}}{H^2}\right) \qquad \text{(D-1)}$$

for

L_{sig} = spectral radiance at the receiver aperture (watts / m^2 sr μm),
D_0 = diameter of receiver aperture (meters),
$\Delta\lambda$ = bandwidth of optical filter (μm),
A_{RES} = area of resolution element on the surface (m^2),
H = sensor altitude, assuming near-nadir pointing (meters).

The number of signal photo-electrons (at the first photo-cathode) per pixel and per exposure time are given by:

$$N_{pe}^{s} = \left(\frac{P_{av}}{h\nu}\right)E\left(T_{filt}T_{lens}\right)\eta \qquad \text{(D-2)}$$

for

hν = energy per photon at wavelength λ (joules), and $h\nu = \frac{hc}{\lambda}$,

E = Exposure time (seconds),

$T_{filt}T_{lens}$ = product of the optical filter and other optics transmission,

η = photo-cathode quantum efficiency at wavelength λ.

Putting these equations together, we re-organize the parameters to find that:

$$N_{pe}^{s} = \left(D_0^2 A_{RES}\right)\left(L_{sig}\lambda\Delta\lambda\eta\right)\left(\frac{\pi E T_{filt} T_{lens}}{4H^2 hc}\right) \qquad \text{(D-3)}$$

Evaluating the equation for the baseline shuttle parameters of

H = 300,000 meters

$T_{filt}T_{lens}$ = 0.5

hc = 2 (10^{-25}) joule-meters,

$$N_{pe}^{s} = 2.2\left(10^{13}\right)\left(E\, D_0^2\, A_{RES}\right)\left(L_{sig}\,\lambda\,\Delta\lambda\,\eta\right). \qquad \text{(D-4)}$$

All the wavelength dependence is contained in the last term:

- L_{sig} is the signal radiance due to the reflected sunlight/skylight from the water and the atmosphere. The values in the Gordon curve (contained in the body of this report) over the wavelength bands of interest are listed in Table D-2
- λ and Δλ in the table are those we selected for the 12 bands (or channels) in order to match up with CZCS and SeaWiFS as well as providing chlorophyll and sediment discrimination, as listed in Table D-1.
- η is the quantum efficiency for the XYBION first photo-cathode, as derived from the responsivity curve for the GEN III Blue implementation in Figure D-1 and the relationship: $R = \frac{\eta e}{\left(hc/\lambda\right)}$ amps/watt. Solving for the quantum efficiency, and putting in the universal constants this implies $\eta = 1.24\left(10^{-6}\right)\frac{R}{\lambda}$.

The wavelength dependent parameters for the 12 bands, as well as their product, are given in Table D-3.

Table D-3. Wavelength Dependent Parameters in Evaluation

Band	λ (meters)	$\Delta\lambda$ (microns)	η	L_{sig} (watts/m^{2}srμm)	Wavelength Factor $L_{sig}\,\lambda\,\Delta\lambda\,\eta$ (watts/m^{2}sr)
1	4.45 (10^{-7})	0.02	0.025	40	8.9 (10^{-9})
2	4.90 "	0.02	0.11	33	3.6 (10^{-8})
3	5.20 "	0.02	0.29	23	5.7 "
4	5.65 "	0.02	0.31	19	6.5 "
5	6.00 "	0.02	0.3	15	5.5 "
6	6.30 "	0.01	0.28	12	2.12 "
7	6.40 "	0.01	0.27	11.5	2 "
8	6.50 "	0.01	0.27	10.3	1.8 "
9	6.65 "	0.01	0.26	10	1.7 "
10	6.85 "	0.01	0.25	9.2	1.57 "
11	7.50 "	0.01	0.21	6.0	9.5 (10^{-9})
12	8.65 "	0.01	0.08	3.2	2.2 "

Bands 11 and 12 are present only for atmospheric radiance correction -- and so pixel averaging can occur in those bands without any loss of information. (There was an additional problem for usage on the shuttle -- the standard shuttle window has very low transmission at the 865 nm region.

The limiting (minimum) value of the wavelength factor is for band 1, the 445 nm band. This is a critical channel, and should be present in any implementation.

We therefore insert the Band 1 value of 8.9 (10^{-9}) watts/m^{2}sr in equation (D-4) and find:

$$N_{pe}^{s} = 1.958\left(10^{5}\right) E\, D_0^2 A_{RES} \qquad \text{(D-5).}$$

For adequate performance (in light of the requirement to make the atmospheric radiance correction and throw away 90% of the signal level in subsequent processing), and assuming signal shot noise limited performance (as discussed in the note at the end of this appendix), we take the required signal level to be $N_{pe}^{s} \geq 250{,}000$ and the system requirement derived from Equation D-5 becomes

$$E\, D_0^2 A_{RES} \geq 1.2 \qquad \text{(D-6).}$$

Writing $A_{RES} = (RES)^2$, then the adequate signal level requirement becomes

Adequate Signal Level Requirement: $E^{1/2} D_0 RES \geq 1.13.$ m^2 [sec]$^{1/2}$

D.2.2 f# Analysis

For the thin lens and small angle approximation, which is appropriate to the XYBION usage contemplated here, the top level optical parameters are related by the formulae;

$$\left(\frac{a}{f}\right)\left(\frac{b}{f}\right)H^2 = A_{RES} = RES_A RES_B \qquad \text{(D-8)}$$

and $f = f^{\#} D_0$

for

a = linear pixel dimension (meters)

b = linear pixel dimension in orthogonal direction (meters)

f = focal length of lens, or, distance from lens to the pixellated photo-cathode, which is assumed to be in the focal plane (meters),

H = shuttle/sensor altitude again, which for a staring receiver oriented at nadir is the same as the sensor-surface range (meters),

A_{RES} = Area of the resolution element on the surface (meter^2),

$RES_{A/B}$ = linear dimension of the resolution element on the surface in the A/B direction (meters),

f# = f-number of the optical lens/mirror system,

D_0 = Diameter of the receiver aperture (meters).

These equations can be manipulated to provide an explicit relation among the parameters:

$$f^{\#} D_0 (A_{RES})^{1/2} = (ab)^{1/2} H = f (A_{RES})^{1/2}. \qquad \text{(D-9)}$$

From the XYBION literature, a=15.8 microns,
b= 18.7 microns,

which means $(ab)^{1/2}$ = 17.19 microns.

Using H = 300,000 meters as the planned shuttle altitude, the remaining parameters are inter-related by the equation:

$$f^{\#} D_0 (A_{RES})^{1/2} = f (A_{RES})^{1/2} = 5.157. \qquad \text{(D-10)}$$

Again using $A_{RES} = (RES)^2$, this relationship can be re-written as

$$f^{\#} D_0 RES = 5.157. \qquad \text{(D-11)}$$

and the requirement for the XYBION pixel size and the shuttle altitude becomes

Pixel Size and STS Altitude Requirement: $D_0 \, RES \leq \left(\frac{5.157}{f^{\#}} \right)$

D.2.3 Consistency Analysis

The two requirements on the (receiver aperture diameter) x (resolution element size) product can be combined to yield

Consistency Requirement: $\frac{1.13}{E^{1/2}} \leq D_0 RES \leq \frac{5.157}{f^{\#}}$ meter^2

The exposure time and resolution element dimension are further related if we add the reasonable constraint that the step and stare "scan" does not miss any areas, i.e. there are no uncovered areas along the direction of flight of the shuttle-based camera. The three key parameters are the speed along the ground of the sub-shuttle point (~ 7.38 km/sec for a shuttle altitude of 300 km), the ~ 700 pixels oriented along the direction of flight, and the desire to sample 12 different wavelength bands for each resolution element through the pre-camera filter wheel.

The view extent along the direction of motion = 700 x RES, and the no-missed -area constraint implies

$$\frac{700 \, RES}{12 \, E} < 7380 \, \frac{m}{\text{sec}} \qquad \text{(D-12)}$$

Solving, $\frac{RES}{E} < 126.5 \, \frac{m}{\text{sec}}$.

For a notional RES = 20 m, this implies $E \geq 0.158$ seconds.

Inserting this into the consistency constraint (again for RES = 20 meters), we find

$$0.142 \leq D_0 \leq \frac{0.258}{f^{\#}} \text{ meters}$$

There is "room" for reasonable aperture sizes if the f# 's are small. The extreme cases are shown in the table:

f#	D_o (meters)
1.0	0.258
1.82	0.142

As a reasonable point design baseline, we choose a 15 cm (6") diameter receiver aperture, and find the consistent set of parameters applies that were listed in subsection D.1 and are reproduced here for completeness.

Shuttle Altitude:	300 km
Optical Aperture Diameter:	15 cm (6 inches)
Optical Transmission:	50%
f# :	1.72
Exposure Time:	158 milli-seconds
Resolution Element:	20 m

The signal levels and (assumed) signal shot noise limited signal to noise ratio for the maximum number of channels (with bandwidths as shown) for the Gordon-radiance levels are shown in Table D-4.

Bands 11 and 12 do not require the 20 meter RES dimension, since they are not really viewing the water at all but the atmospheric radiance. Hence, their SNR can be substantially increased by pixel averaging.

Note: Signal Shot Noise Limited Operation

The receiver will be signal shot noise limited if the dark current is negligible compared to the signal counts in Table D-4, since the micro-channel plate within the front-end tube provides nearly noiseless gain of ~ 10^6. This note estimates the expected value of dark counts, if all dark counts originate at the photo-cathode. This is valid because all other dark counts in the camera system will undergo far less gain, and when rendered in terms of equivalent photo-electrons at the cathode, will be negligible.

The XYBION tube selected has a Gen-III blue photo-cathode, with significant response out into the near infra-red. We used two different types of such tubes in the ARFORM work on the Navy Blue-Green program, and found that at room temperature the dark current density was of order 1 to 2 (10^{-14}) amps/cm^2 .

Table D-4 Performance of Staring XYBION Camera from Shuttle Altitudes

Band or Channel	Wavelength (nm)	Channel Bandwidth (nm)	Signal Photo-electrons per pixel per exposure time (of 158 milliseconds)	Signal-to-Noise Ratio
1	445	20	278,412	528
2	490	20	1,220,076	1105
3	520	20	1,783,188	1335
4	565	20	2,033,460	1426
5	600	20	1,720,620	1312
6	630	10	675,354	822
7	640	10	628,680	791
8	650	10	563,112	750
9	665	10	531,328	729
10	685	10	491,159	701
11	750	10	297,198	545
12	865	10	68,825	262

The generic equation for the number of dark counts arising on the average for a given dark current density, area, and time interval is given by:

$$N_{pe}^{dc} = \frac{I_{dc} A_{px} \Delta t}{e}$$

for I_{dc} = dark current density, amps/cm^2 ;
A_{px} = Area of interest, here the area of one pixel, cm^2;
Δt = time interval of interest, here the exposure time (seconds);
e = charge on the electron, = 1.6 (10^{-19}) coulombs.

The dark counts for a XYBION pixel during a single frame are estimated in the worst case from

I_{dc} = 10^{-13} amps/cm^2 ;
A_{px} = [17 microns]^2 = 2.89 (10^{-6}) cm^2;
Δt = 158 (10^{-3}) seconds.

The result: N_{pe}^{dc} = 0.28 per pixel per exposure time.

This is clearly negligible compared to the > 65,000 signal photo-electrons in even the least responsive of the bands, so the camera system can be taken as signal shot noise limited.